ACS Biomaterials SCIENCE & ENGINEERING
Article
Cite This: ACS Biomater. Sci. Eng. 2019, 5, 2899−2915
pubs.acs.org/journal/abseba

Development of Dual Drug Eluting Cardiovascular Stent with Ultrathin Flexible Poly(L-lactide-*co*-caprolactone) Coating

Purandhi Roopmani,[†,‡] Santhosh Satheesh,[∥] David C. Raj,[‡] and Uma Maheswari Krishnan*[,†,‡,§]

[†]Centre for Nanotechnology & Advanced Biomaterials (CeNTAB), [‡] School of Chemical & Biotechnology, and [§]School of Arts, Science & Humanities, SASTRA Deemed University, Thanjavur−613401, Tamil Nadu, India

[∥]Department of Cardiology, Jawaharlal Institute of Post Graduate Medical Education and Research (JIPMER), Pondicherry−605006, India

Supporting Information

ABSTRACT: The pleiotropic effects of the atorvastatin−fenofibrate combination can be effectively harnessed for site-specific therapy to minimize stent-related complications. The present study aims to utilize the pleiotropic effects of these two drugs entrapped in a uniform and defect-free coating of poly(L-lactide-*co*-caprolactone) (PLCL) on a stainless steel stent to overcome stent-associated limitations. The stent coating parameters were optimized using ultrasonic spray coating technique to achieve a thin, smooth, and defect-free dual drug-loaded polymer coating on the stent. The dual drug-loaded polymer coated stent was characterized for surface morphology, thickness and coating integrity. *In vitro* drug release kinetics of the fabricated stent reveals a sustained release of both drugs for more than 60 days. Significant reduction of thrombus formation and adhesion of lipopolysaccharide-stimulated macrophages on the dual drug containing polymer-coated stent indicates that the drug combination possesses antithrombotic and anti-inflammatory effects. The combination did not adversely influence endothelialization but significantly retarded smooth muscle cell proliferation indicating its potential to overcome restenosis. No bacterial biofilm formation was observed on the stent due to the antibacterial activity of atorvastatin. A rat subcutaneous model was used to evaluate the biocompatibility of the coated stent and compared with the commercial stent. MicroCT, scanning electron microscopy, and morphometric analyses revealed that the coated stents exhibited excellent histocompatibility with no inflammatory response as evidenced from the cytokine levels measured 28 days postimplantation. Our data demonstrates for the first time that the combination of atorvastatin and fenofibrate can be successfully employed in cardiovascular stents to overcome the current limitations of conventional drug-eluting stents.

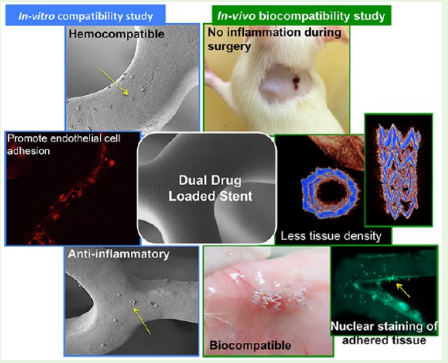

KEYWORDS: *dual drug-eluting stent, ultrasonic spray technique, in vivo biocompatibility, atorvastatin−fenofibrate*

1. INTRODUCTION

Drastic changes in lifestyle, dietary habits, and environment quality in the modern era have resulted in increased incidence of atherosclerosis across the globe.[1] The extensively employed therapeutic intervention for this condition is the deployment of stents at the blocked site to restore circulation through the blood vessels.[2] Regardless of the success and advancement in stent technology, recurrence of restenosis and late stent thrombosis continue to limit the performance of coronary interventions. Restenosis arises due to imbalance in the proliferation rates of endothelial and smooth muscle cells whereas thrombosis occurs due to adhesion and activation of the platelets by the stent surface.[3,4] Conventionally, drug-eluting stents containing antiproliferative drugs such as sirolimus, everolimus, paclitaxel, *etc.*, have been employed in combination with antiplatelet agents such as clopidogrel, aspirin, dabigatran, rivaroxaban, etc.[5] The past generations of drug-eluting stents have clinically proven their efficiency in reducing the in-stent restenosis by 20%.[6] However, though the antiproliferative drugs retard the migration and proliferation of human vascular smooth muscle cells, they also lead to poor endothelialization thereby initiating the prothrombotic cascade and escalation of inflammatory responses.[7] In addition, long-term antithrombotic therapy causes several adverse effects, especially bleeding risks, thereby lowering the quality of life.[8] To mitigate stent-associated complications, new drugs, nano-textured stent surfaces, bioresorbable platforms, and other surface functionalization techniques have been explored.[9] However, such expensive and complex strategies produced less satisfactory results in clinical trials. Further, epidemiological variations in the therapeutic outcomes have also been reported.[10]

Due to the shortcomings of monotherapy employed in conventional drug-eluting stents, combinations of drugs have been explored as an alternative. Blends of antiproliferative drugs with antithrombotic or re-endothelialization promoter[11]

Received: March 2, 2019
Accepted: April 10, 2019
Published: April 10, 2019

DOI: 10.1021/acsbiomaterials.9b00303
ACS Biomater. Sci. Eng. 2019, 5, 2899−2915

have been explored for use in multidrug eluting stents. The choice of therapeutic agents and their release kinetics from the coating employed influences the performance of the multidrug eluting stents. Many combinations such as r-PEG-hirudin and iloprost,[12] paclitaxel and pimecrolimus,[13] sirolimus and estradiol,[14] paclitaxel and cilostazol,[15] sirolimus and paclitaxel,[16] *etc.*, have been attempted but had low success in clinical trials. The clinical trials revealed that there was no significant reduction in the thrombosis events using the above combinations.[11] The fast release of drugs from the stent could have been a probable reason for the lack of significant antithrombotic activity. Several other combinations are also being investigated but clinical trial data is not yet available.[11] Moreover, the lack of specificity manifested through poor wound healing at the stented site is another drawback of typical antiproliferative drugs used in coronary stents.[17] Therefore, it is evident that an ideal combination of multiaction drugs should possess specific inhibitory action toward vascular smooth muscle cells apart from exhibiting endothelial cell-protective, anti-inflammatory, and antithrombotic effects. In this context, the present work explores the combination of two well-known lipid-lowering drugs atorvastatin and fenofibrate that have been reported to exert beneficial effects on cardiovascular alignment through nonlipid lowering mechanisms,[18] but have never been studied earlier as a combination in coronary stents.

Atorvastatin, a HMG-CoA (hydroxymethyl glutaryl-coenzyme A) reductase inhibitor, has been shown to inhibit the activation and invasion of vascular smooth muscle cells by regulating various intracellular signaling pathways such as NFκB (nuclear factor κ-B),[19] RhoA-Rho related kinase,[20,21] and other small GTPase family proteins.[22] Moreover, it has been found to exhibit a stabilizing effect against vascular injury caused by chemo-attractants like platelet-derived growth factor-BB.[23,24] Other important pleiotropic effects of atorvastatin include its ability to elevate eNOS (endothelial nitric oxide synthase) and expression levels of endothelial junction proteins,[25,26] escalate nitric oxide production, and regulate Akt/PKB (protein kinase B) signaling[27] in endothelial cells. Atorvastatin has also been shown to retard atherosclerosis-induced release of pro-inflammatory cytokines.[28,29] These pleiotropic properties suggest that atorvastatin can counter endothelial dysfunction.

Fenofibrate, a peroxisome proliferator-activated receptor-α (PPAR-α) activator, exerts anti-inflammatory effect against vascular smooth muscle cell (VSMC) induced interleukins.[30] This property may be beneficial in lowering the risk of implant-based inflammation. An earlier report has described the inhibition of VSMC synthesis stimulated via platelet-derived growth factor (PDGF) by treatment with fenofibrate.[31] Fenofibric acid, an active form of fenofibrate has been found to retard the activity of PDGF independent of cholesterol mechanism. Also, fenofibrate exhibits an anti-atherogenic effect on vascular smooth muscle cells by decreasing the biosynthesis of proteoglycans.[32] Further, it has been demonstrated to significantly decrease arterial thrombus formation and platelet aggregation in animal models by inhibiting thromboxane A_2 receptor and cyclooxygenase-1.[33] Fenofibrate also prevents endothelial dysfunction by increasing antioxidant-mediated production of the vasodilator nitric oxide.[34] Though both drug molecules have independently and in combination displayed cardio-protective properties, they have never been considered as a possible combination for stent-based delivery. The present work for the first time aims to fabricate, optimize and characterize a polymer coating containing the two lipid-lowering drugs over a metallic stent and evaluate its *in vivo* biocompatibility. The biodegradable polyester poly(L-lactide-*co*-caprolactone) (PLCL) (70:30) was chosen as the polymer matrix over the commonly employed PLGA (poly(lactide-*co*-glycolide). This is because PLGA coatings are more prone to brittle fracture depending on their lactide content that may lead to complications during crimping and stent deployment.[35] PLCL is a biocompatible polyester that has been employed for tissue engineering applications and exhibits controlled degradation and elastic nature,[36] both of which are valuable for stent applications.

2. MATERIALS AND METHODS

2.1. Materials. Poly(L-lactide-*co*-ϵ-caprolactone) (7030LCL MW = 230 kDa) was purchased from Evonik Degussa Corporation (Birmingham, USA). Atorvastatin calcium (ATS) (MW = 1209.4 g/mol) was obtained from Swapnroop Drugs & Pharmaceuticals (India) and fenofibrate (FF) (F6020 MW = 360.83 g/mol) was purchased from Sigma-Aldrich (USA). Acetone of HPLC grade from Merck, India, was used to dissolve the polymer and drugs. All organic solvents and chemicals used were of analytical grade. All metal stents (316L stainless steel, 7 mm in length) and stent delivery catheters were provided by JIPMER (Pondicherry, India) for optimizing the stent coating. For *in vivo* study, the commercial stents and bare metal stents were gifted by an Indian stent manufacturer. The multianalyte ELISA kit was purchased from Qiagen, USA.

2.2. Fabrication of Dual Drug Loaded PLCL Stents. MediCoat (DES1000, Sono-Tek Corporation, Milton, NY), a customized ultrasonic spray system, was used for coating the bare metal stent. The stainless steel stents (length 7 mm, diameter 3 mm) were cleaned with acetone and distilled water, air-dried, and mounted on a mandrel of 3 mm diameter. For spray coating, 3% of PLCL and drugs (1:1 ratio) were dissolved in HPLC grade acetone and loaded in a syringe pump. The drug ratio was chosen based on our earlier *in vitro* studies using human umbilical vein endothelial cells (HUVECs) and human vascular smooth muscle cells (hVSMCs). The flow rate, ultrasonic power, gas pressure, distance between nozzle and stent, rotation speed, and other coating parameters were thoroughly examined for obtaining a defect-free smooth coating. After coating, stents were vacuum-dried for 2 days. Surface morphology of the coated stents was observed under field emission scanning electron microscopy (FE-SEM, JSM 6701F, JEOL, Japan).

2.3. Balloon Expansion Test. The quality and integrity of therapeutic coating were evaluated using balloon expansion test. Dual drug coated stents were manually compressed on a balloon catheter up to a diameter of 1 mm. After imaging, crimped stents were then expanded to 3 mm diameter by applying a pressure of 12 psi. The morphology of the coating after the expansion was examined by using FE-SEM (JSM 6701F, JEOL, Japan).

2.4. *In Vitro* Drug Release Study. Drug release studies on the dual drug-loaded PLCL stents (n = 3) were performed in PBS (phosphate buffered saline) medium (pH 7.4) at 80 rpm for 80 days at 37 °C. The medium was collected and replaced with fresh medium at every time point. The collected medium was analyzed using UV−visible spectrophotometry (Lambda 25, PerkinElmer, USA) at 246 and 286 nm for atorvastatin and fenofibrate, respectively. To observe the morphological changes in the coating after 80 days of drug release, the surface of the stents was imaged using SEM (TESCAN Vega, Czech Republic).

2.5. *In Vitro* Degradation Study. Dual drug-loaded PLCL coated stents were incubated in PBS (pH 7.4) at 37 °C under constant stirring at 80−120 rpm. The medium was replaced with fresh medium every alternate day. At specific time points, the stents were removed, rinsed with distilled water, air-dried, and subjected to vacuum drying. The change in surface morphology of the stent coated with dual drug loaded polymer was imaged using SEM.

DOI: 10.1021/acsbiomaterials.9b00303
ACS Biomater. Sci. Eng. 2019, 5, 2899−2915

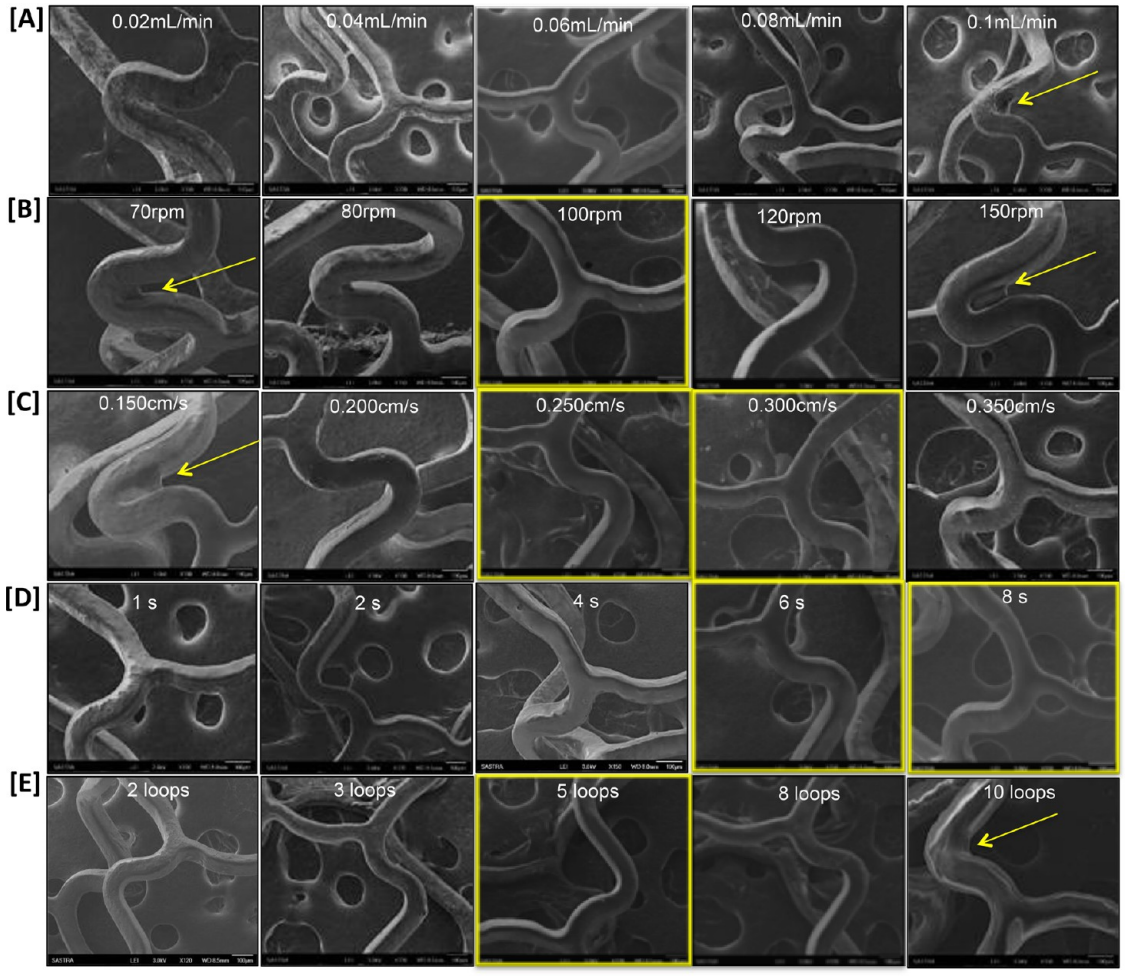

Figure 1. Scanning electron micrographs of the surface of PLCL coated stent depicting the effect of various conditions during optimization of different coating parameters [A] flow rate, [B] rotation speed, [C] translation speed, [D] delay time, and [E] number of loops. The scale bar represents 100 μm. The arrows show the coating defects.

2.6. Cell Adhesion Study and Immunostaining. Human umbilical vein endothelial cells (HUVECs) (Hi-Media, India) were cultured in endothelial growth medium-2 EGM-2 (Lonza, USA) and human vascular smooth muscle cells (hVSMC) were maintained in Dulbecco's modified Eagle's medium (DMEM) (Gibco, USA) supplemented with 10% fetal bovine serum, 1% penicillin-streptomycin at 37 °C, and incubated in 5% CO_2 (NU-8500, Nuaire, USA). For the study, bare stainless steel stents and dual drug-loaded PLCL coated stents were UV sterilized and incubated with 50 000 cells per well. At days 1 and 3, the morphology of adhered HUVEC and hVSMC was observed using SEM after fixing the cells using 2.5% glutaraldehyde. For immunostaining, the adhered cells were fixed using paraformaldehyde (4%) for 10 min followed by TritonX-100 (0.3%) in PBS buffer for 10 min at room temperature. The samples were then incubated for 1 h using blocking solution (1% bovine serum albumin). Postincubation, samples were washed with DPBS followed by overnight incubation with antibodies against endothelial cell adhesion molecule (CD31) (Abcam, USA) and α-SMA (alpha-smooth muscle cell actin) (1:100) (Abcam, USA) at 4 °C. This was followed by removal of primary antibody. The samples were washed with DPBS and incubated with goat antimouse IgG (H+L) Alexa Fluor 555 (Invitrogen, USA) for 1 h. The samples were then observed using fluorescence microscopy (Nikon Eclipse, TS100, Japan).

2.7. Whole Blood Adhesion and APTT Test. The dual drug loaded PLCL stent was further tested for *in vitro* hemocompatibility using whole blood. The bare stainless steel stent, PLCL coated stent, and dual drug-loaded PLCL coated stent were incubated with freshly collected human blood for 1 h at 37 °C under static conditions. After incubation, the stents were washed gently with phosphate buffered saline, and the adhered cells were fixed by by overnight incubation with 2.5% glutaraldehyde followed by dehydration of the stents by sequential treatment using 50%, 70%, 90%, and 100% ethanol. After fixing, the stents were vacuum-dried and imaged using FE-SEM. To evaluate the *in vitro* anticoagulation property, the APTT (activated partial thromboplastin time) test was performed using blood plasma. Bare metal, PLCL coated, and dual drug-loaded PLCL coated stents (n = 3) were incubated with100 μL of freshly isolated platelet poor plasma for 15 min at 37 °C. After incubation, 100 μL of cephaloplastin reagent was added followed by $CaCl_2$ solution (0.025 M). The sample was left undisturbed for 3 min. The time taken for the appearance of a fine thread of clot was measured using coagulometer (STA Compact Stago, USA). The results were compared with those obtained for platelet poor plasma.

2.8. *In Vitro* Inflammatory Response. Stent samples were cultured with IC-21 mouse macrophage cell line (NCCS, Pune) stimulated with 100 ng/mL of lipopolysaccharide (LPS) (Sigma-Aldrich, USA) to test their anti-inflammatory response. Cells were maintained in RPMI medium (Invitrogen, USA) with 10% FBS and 1% penicillin−streptomycin (Gibco, USA). LPS-stimulated IC-21 cells with the seeding density of 50 000 cells per well were incubated with bare stainless steel or PLCL coated or dual drug-loaded PLCL coated stents for 24 h. The cell morphology was observed under phase contrast microscopy (Zeiss Axio Vert A1, USA). Further, the cells adhered to the surface of the stents were fixed with 2.5% glutaraldehyde and imaged using SEM.

DOI: 10.1021/acsbiomaterials.9b00303
ACS Biomater. Sci. Eng. 2019, 5, 2899−2915

2.9. Biofilm Formation. Sterilized stents were incubated with tryptic soy broth (TSB) (Hi-Media, India) inoculated with 2% bacterial culture of *Staphylococcus aureus* (ATCC 25923). After 24 h of incubation, stents were washed with PBS and the adhered bacteria were fixed with 2.5% glutaraldehyde and observed using scanning electron microscopy.

2.10. *In Vivo* Studies. *In vivo* biocompatibility of the dual drug-loaded PLCL stent was tested by subcutaneous implantation in *Wistar* rats. All animal experiments were carried out after approval of the study protocol from the Institutional Animal Ethics Committee (471/SASTRA/IAEC/RPP). Twenty-four male *Wistar* rats about 6−8 weeks old were chosen for the study. They were segregated and acclimatized before the surgery. Animals were anaesthetized using ketamine (80 mg/kg ip) (Aneket, Neon Laboratories, India) and xylazine (6 mg/kg ip) (Tamil Nadu Government supplies, India). The hair was removed from the dorsal side of the rats and the skin was sterilized with 70% ethanol. A small incision was made to expose the dorsum. A deep subcutaneous pouch was created using sterile surgical scissors. Ethylene oxide (ETO) sterilized stents were implanted in the pouch using 1 mL sterile syringe. Once the stent was secured in the subcutaneous pouch, the incision was closed with sterile absorbable surgical sutures (ETHICON, Johnson & Johnson, India) and povidone iodine was applied near the suture.

2.11. Micro-CT Analysis. X-ray scans of the implanted sites were taken on the 7th and 28th days post-stenting using a Micro-CT SKYSCAN (Bruker, Germany). Animals with commercial and dual drug-loaded PLCL coated stents were anaesthetized and prepared for the scan. Each animal was scanned for 180°, and a three-dimensional visualization was obtained by enhancing the contrast using the Micro-CT software (CTVox).

2.12. Necropsy. After 7 and 28 days of stent implantation, the animals were euthanized using the CO_2 inhalation method and the skin was cut open to expose the site of stent implantation. Images of the subcutaneous pocket with the stent were taken. Stents along with surrounding tissue were isolated and carefully stored in 10% neutral buffered formalin solution for histopathological analysis. To analyze the tissue adhesion and stent coating quality, the samples were fixed with 2.5% glutaraldehyde and imaged using SEM (TESCAN Vega, Czech Republic).

2.13. Quantification of Inflammatory Cytokines. Multi-Analyte ELISA kit (Qiagen, USA) was used to detect the levels of inflammatory markers in the serum collected from the animals before euthanasia. The kit quantifies the cytokines like interleukin 1A (IL-1A), interleukin 1B (IL-1B), interleukin 2 (IL-2), interleukin 4 (IL-4), interleukin 6 (IL-6), interleukin 8 (IL-8), interleukin 10 (IL-10), interleukin 12 (IL-12), interleukin 17A (IL-17A), and interferon γ (IFN-γ), tumor necrosis factor α (TNF-α), granulocyte macrophage-colony stimulating factor (GM-CSF), and regulated on activation, normal T cells expressed and secreted (RANTES), which are involved in inflammation and T-cell biology. This assay was used to evaluate inflammation caused by the dual drug eluting stent and was compared with sham control. Following the manufacturer's protocol, 50 μL of serum samples collected from animals 28 days post-stenting or standards were added to appropriate wells. The samples were incubated for 2 h at room temperature. After washing, 100 μL of detection antibody solution was added and incubated for 1 h. After incubation, the strips were washed 4 times using the washing buffer and 100 μL avidin−HRP solution was added and incubated at room temperature for 30 min. Finally, 100 μL of the development solution was added to each well and incubated in the dark for 15 min at room temperature. Subsequently, 100 μL of stop solution was added to each well, and the absorbance of the samples was measured at a wavelength of 450 nm using a multimode reader (Infinite M200, Tecan, Austria).

2.14. Statistical Analysis. The results of all experiments performed in triplicate were analyzed using one-way ANOVA. The statistical significance (* $p < 0.05$) was determined using student-t test.

3. RESULTS AND DISCUSSION

3.1. Stent Coating. Irregularities in stent coating can cause serious complication of thrombosis within 24 h of stent implantation. Hence it is very important to develop a smooth and uniform therapeutic coating on the stents without any defects. FE-SEM images (Figure 1) of polymer coated stent show the effect of various coating parameters on surface morphology and uniformity of the coating. The complete coverage of the stent with smooth surface was observed at 3 wt % polymer solution which was selected for further trials. Similarly, 1.5 W of ultrasound frequency, 0.5 psi of gas pressure and 6 mm distance between nozzle and stent were optimized based on a uniform shape of the spray of the polymer solution and formation of a uniform coating on the surface with less defects. These conditions were kept constant while optimizing major stent coating parameters. Figure 1A shows the SEM images of the stent coated at various flow rates from 0.02 to 0.1 mL/min while the rotation speed, feeding speed, and delay time was kept constant at 100 rev/min, 0.300 cm/s, and 2 s, respectively, with the number of loops kept at 2. At a low flow rate of 0.02 mL/min, the spray was unable to cover the entire stent while at the high flow rate of 0.1 mL/min webbing defects were formed near the struts due to a large amount of polymer deposition. Moderate flow rates did not show defects, but based on the smoothness of the coating, the flow rate of 0.06 mL/min was chosen as optimum. The rotation speed of the stent was varied from 70 to 150 rpm for obtaining a defect-free coating, with the flow rate maintained at 0.06 mL/min, feeding speed at 0.300 cm/s, delay time at 2 s, and number of loops at 2. Both low as well as high rotation speeds, resulted in webbing defects (Figure 1B). At 100 and 120 rpm no defects were observed but depending on better surface uniformity, 100 rpm was chosen as optimum for a smooth coating. Feeding or translation speed that defines the movement of the stent from one position to another under the spray was varied from 0.150 to 0.350 cm/s at 0.06 mL/min flow rate, 100 rpm rotation speed, delay time of 2 s, and 2 cycles. Webbing defects were noticed at a low speed of 0.150 cm/s due to excessive deposition of polymer, whereas at 0.200 cm/s an uneven coating was observed. At a high feeding speed of 0.350 cm/s, the coated surface was rough because of the nonuniform evaporation of the solvent. Therefore, 0.250 and 0.300 cm/s with minimum inhomogeneity and defects were chosen for further trials. The delay time between each loop of the stent was varied from 1 to 8 s. Based on the uniform and smooth coating obtained, 6 and 8 s were chosen for further trials. Finally, the number of loops was examined from 2 to 10 loops at a flow rate of 0.06 mL/min, rotation speed of 100 rpm, feeding speed of 0.300 cm/s, and delay time of 2 s. For 5 loops, an even smooth coating with the thickness of 1 μm was obtained, and this was chosen as the optimum value.

Based on the initial optimization trials, two different sets of conditions with different feeding speed and delay time were shortlisted for single drug coating. The drug-loaded polymer coating was evaluated using FE-SEM. Results revealed that feeding speed of 0.300 cm/s, flow rate of 0.06 mL/min, rotation speed of 120 rpm, 5 loops, and delay time of 8 s show no phase separation and formed a uniform coating due to steady evaporation of solvent and, therefore, were selected for dual drug coating (Supporting Information. Figure S1, FE-SEM images of drug loaded stents at different coating conditions).

DOI: 10.1021/acsbiomaterials.9b00303
ACS Biomater. Sci. Eng. 2019, 5, 2899−2915

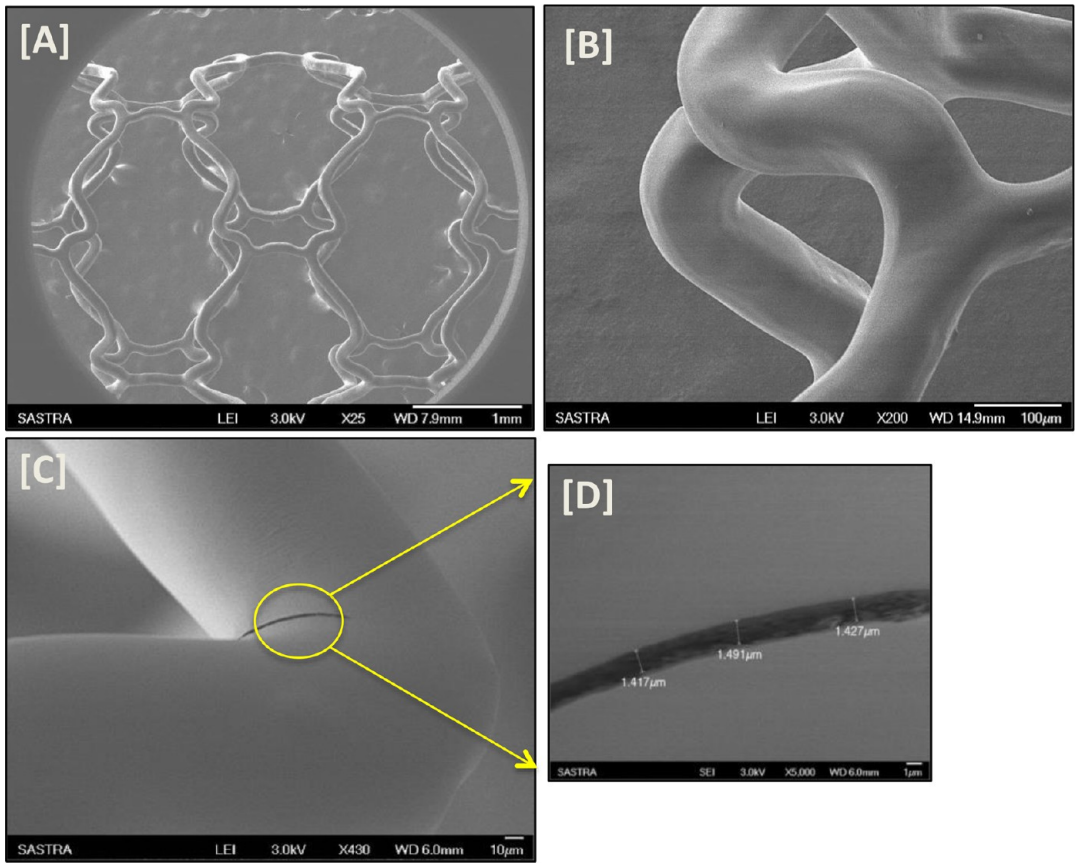

Figure 2. FE-SEM of dual drug-loaded PLCL coated stent at [A] low magnification and [B] at high magnification using optimized coating parameters, [C] scratch test to measure the thickness of drug-loaded polymer coating and [D] Thickness of coating at high magnification with annotation.

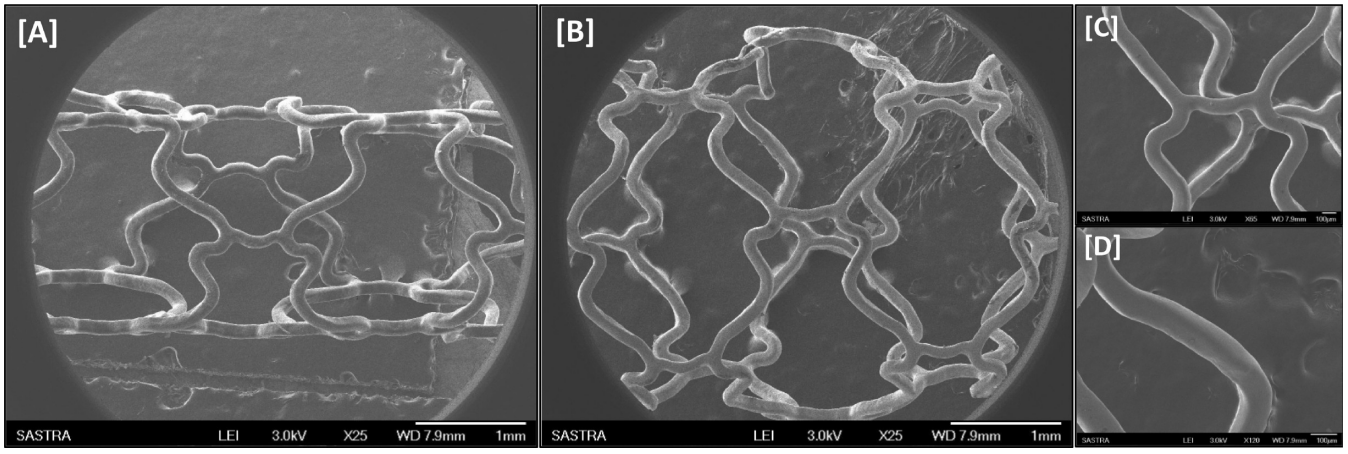

Figure 3. FE-SEM images of dual drug-loaded PLCL coated stent [A] before balloon expansion (crimped position) and [B] after balloon expansion test. [C and D] High magnification images of the stent after expansion. Scale bars for C and D represent 100 μm.

Figure 2 shows the FE-SEM images of the stent with smooth and wrinkle-free dual drug-loaded polymer coating without any coating defects. The optimized therapeutic coating was further characterized for its stability and tested for hemocompatibility before the *in vivo* biocompatibility study. The scratch test performed on the coating to measure the coating thickness revealed that the dual drug-loaded polymer coating thickness was 1.4 μm, which is comparatively thinner than the coatings in commercially available drug-eluting stents, which are about 5−6 μm thick.[37] The thinner layer of the polymer will ensure the least obstruction to blood flow through the stented vessels.

The ultrasonic spray technique involves translation and rotational movements of the stent, which ensures uniform coverage in both planar and nonplanar regions of the stent by the ultrafine mist of the polymer spray.[38] The thickness of the coating is in turn determined by the density of spray that is optimized through controlling the feed rate of the gas and liquid in to the spray nozzle. A uniform droplet size spray increases the uniformity of the coating thickness.[39]

DOI: 10.1021/acsbiomaterials.9b00303
ACS Biomater. Sci. Eng. 2019, 5, 2899−2915

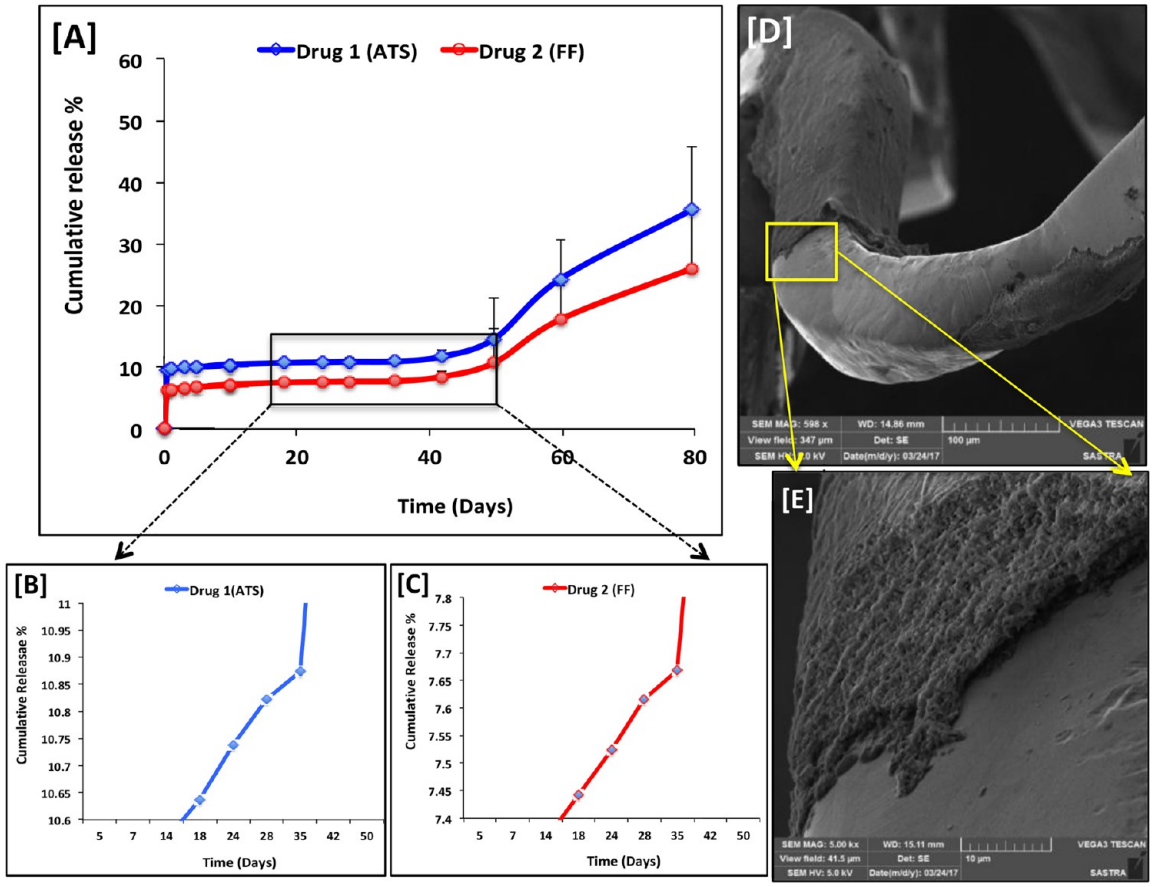

Figure 4. [A] *In vitro* drug release profiles of atorvastatin and fenofibrate from the dual drug-loaded PLCL coated stent. [B and C] Expanded plots of the release. [D] SEM of dual drug-loaded PLCL coated stent at low and [E] high magnification after 80 days of release.

Table 1. Regression Coefficients of Various Mathematical Models of Drug Release at Different Time Points[a]

	overall (0–80 days)		0–72 h		0–42 days		42–80 days	
models	ATS	FF	ATS	FF	ATS	FF	ATS	FF
zero order	0.6569	0.7150	NC	NC	NC	NC	0.6465	0.6400
first order	0.6733	0.7245	NC	NC	NC	NC	0.6679	0.6608
Higuchi	0.7441	0.7594	NC	NC	NC	NC	0.5271	0.5228
Korsmeyer–Peppas	0.7503	0.7764	0.5702	0.6734	0.8910	0.9214	0.6552	0.6490
Hixson–Crowell	0.6696	0.7222	NC	NC	NC	NC	0.6677	0.6578
Hopfenberg	0.6733	0.7244	NC	NC	NC	NC	0.6685	0.6605
Baker–Lonsdale	0.7338	0.7512	NC	NC	NC	NC	0.5018	0.5057
Makoid–Banakar	0.8683	0.8798	0.7270	0.7754	**0.9441**	**0.9539**	**0.9563**	**0.9524**
Peppas–Sahlin	0.7709	0.7962	0.7814	0.8188	0.8923	0.9229	0.7400	0.7335
quadratic	0.6739	0.7261	NC	NC	NC	NC	0.6718	0.660
Weibull	**0.8636**	**0.8737**	**0.9634**	**0.9971**	**0.9350**	**0.9489**	0.9177	0.9118
logistic	0.7185	0.7556	0.5725	0.6745	0.8899	0.9205	0.6935	0.6737
Gompertz	0.6541	0.6932	0.5796	0.6813	0.8865	0.9166	0.7317	0.7088
Probit	0.6896	0.7258	0.5760	0.6782	0.8882	0.9185	0.7046	0.6868

[a]NC (not correlated).

3.2. Balloon Expansion Test. An important requirement of polymer coating over stents is their flexibility. The stents are generally crimped over the balloon and are then expanded during the deployment. The polymer coating should withstand these extreme changes in pressure and deformative stresses without undergoing any brittle fractures. The presence of drug molecules in the polymer matrix may also alter the flexibility of the polymer film. To characterize the flexibility of the dual drug-loaded PLCL coating, a balloon expansion test was performed. It was found that the dual drug-loaded PLCL coating displayed no cracking or peeling after the crimping and expansion cycle (Figure 3) indicating that the presence of both drugs in PLCL film did not alter its adhesion or flexible nature. At higher magnification, a smooth and uniform coating was observed without any microdefects or delamination suggesting that the drug-loaded polymer coating possesses sufficient elasticity that can remain stable even after the expansion stress. This finding augers well for the use of this dual drug-loaded

DOI: 10.1021/acsbiomaterials.9b00303
ACS Biomater. Sci. Eng. 2019, 5, 2899–2915

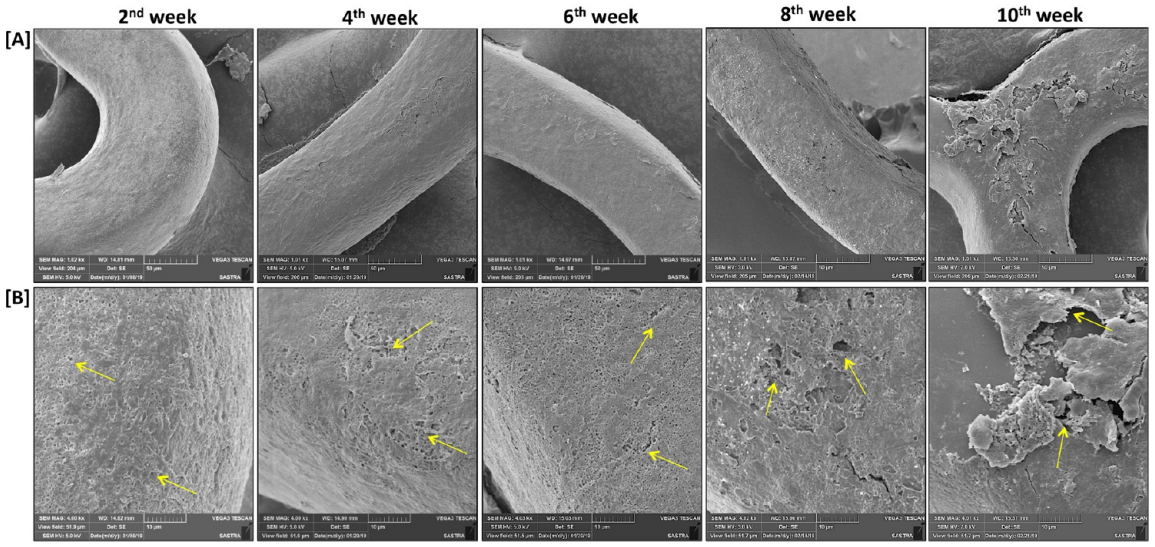

Figure 5. SEM images of dual drug loaded stent surface during *in vitro* degradation study at [A] low and [B] high magnification.

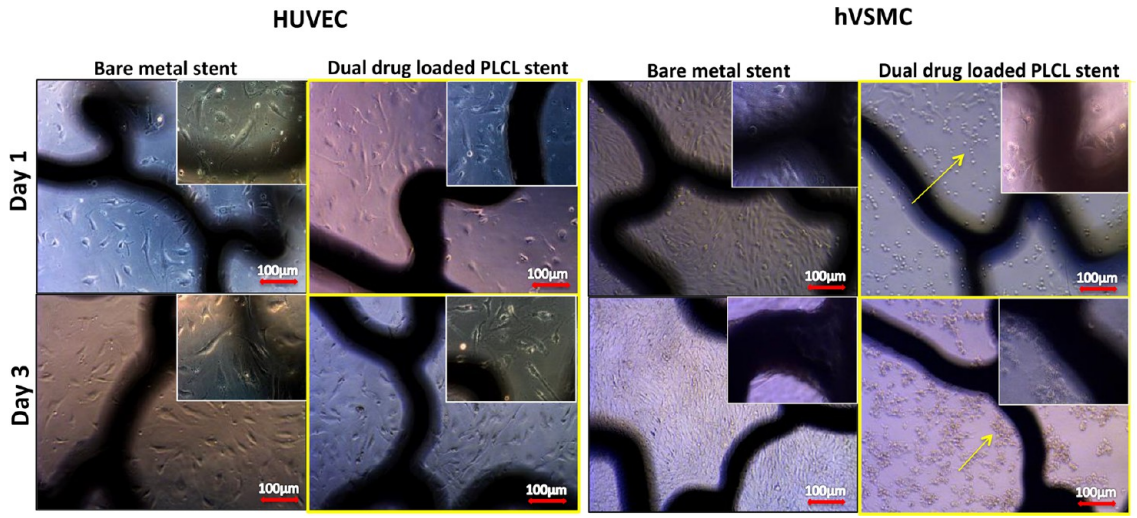

Figure 6. Phase contrast microscopy images of HUVEC and hVSMC cultured with the bare metal stent and dual drug eluting stent.

polymer as a therapeutic coating on stents, which may undergo repeated deformation.[40]

3.3. *In Vitro* Release Profile. The release profile of both drugs from the polymer coating was investigated at 37 °C in PBS under the dynamic condition at 80 rpm, and the results are presented in Figure 4. A sustained release was observed for both drugs over a period of 80 days. The cumulative release of atorvastatin was higher when compared to fenofibrate at all the time points. Fenofibrate is uncharged while atorvastatin is anionic, and this difference may influence the distribution of the two drugs within the PLCL matrix. The atorvastatin may prefer to localize toward the periphery while the fenofibrate partitions into the interior. This accounts for the higher burst release observed in the case of atorvastatin. SEM images of this therapeutic coating on stents after 80 days reveal that the coating is still present on the stent but with a rough surface morphology (Figure 4). This indicates that the polymer film has degraded slowly. Mathematical modeling of the drug release kinetics over 80 days was performed, and the regression coefficients were calculated from the standard equations (Table 1).

It is observed that the release profiles of both atorvastatin and fenofibrate did not agree with most of the kinetic models over the total 80-day period. The closest agreement was with the Weibull model that describes the release from a matrix-based system. This suggests that the drug release is controlled by different parameters at different time points. When the drug release profiles were modeled for specific time points, the initial release up to 72 h was found to agree with the Weibull kinetics for both drugs while, at later time points, the Makoid–Banakar model and Weibull kinetics were in close agreement with the release profiles suggesting that a diffusion-erosion mechanism was in operation. Considering the hydrophobic nature of the drugs, the release study was carried out maintaining sink conditions by addition of 10% solvent in the release medium.[41,42] The drug release in drug eluting stents is influenced by many factors such as coating morphology, heterogeneous drug distribution, drug nature, degradation rate of polymer, etc.[43] In the present study, the differential localization of the two drugs in the polymer film may contribute to the difference in the release rates of the two drugs, especially in the initial time points. Atorvastatin is preferentially localized on the surface while fenofibrate

DOI: 10.1021/acsbiomaterials.9b00303
ACS Biomater. Sci. Eng. 2019, 5, 2899–2915

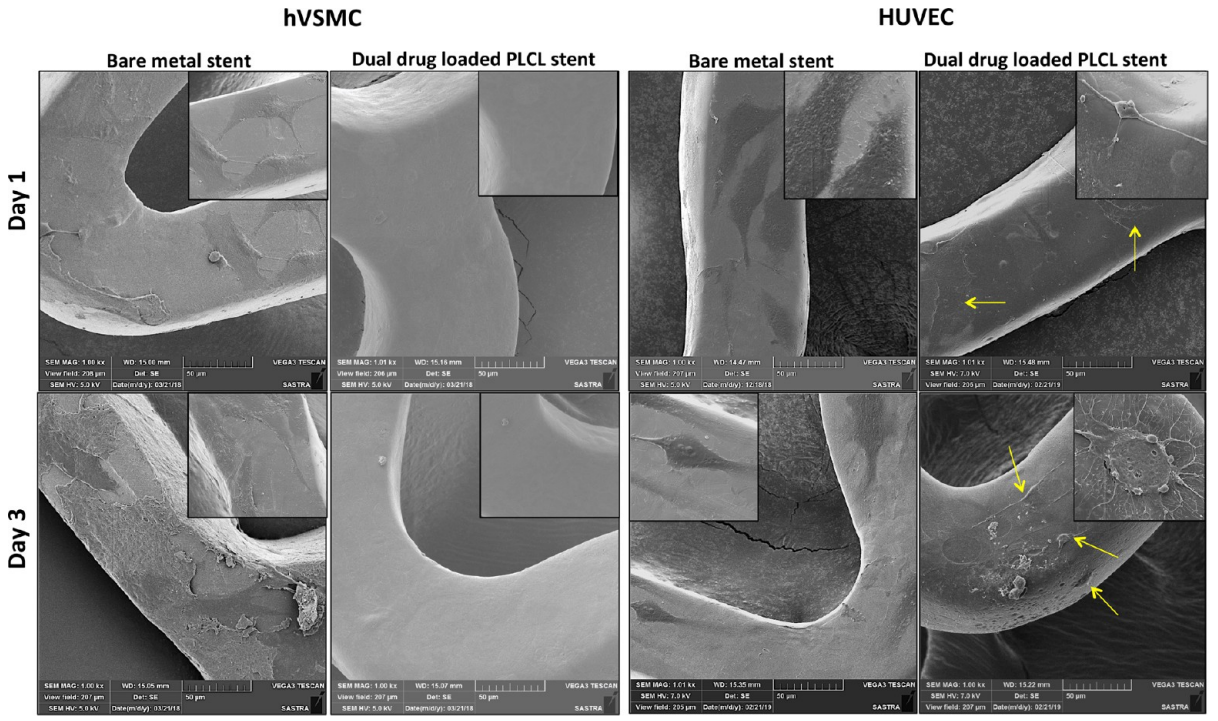

Figure 7. SEM images of bare metal and dual drug loaded stents after culture with hVSMC and HUVEC for 3 days. Scale bars represent 50 μm, and 20 μm for the insets.

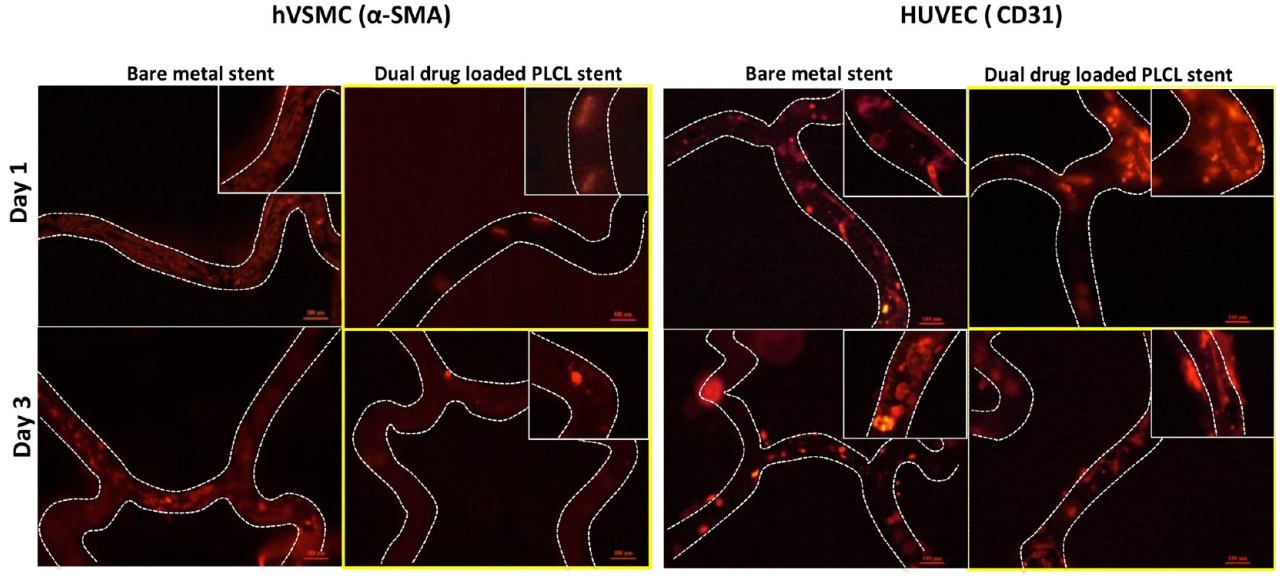

Figure 8. Fluorescence microscopy images of α-SMA and CD31 staining on adhered hVSMC and HUVEC respectively on bare metal and dual drug-loaded PLCL coated stents. Scale bars represent 100 μm.

partitioned deeper into the polymer film. This is also reflected in the higher burst release (7%) for atorvastatin when compared to fenofibrate (4.6%). The burst release of the drugs was observed in first 2−6 h of release, which is followed by a period of sustained release. The burst release is attributed to the drug present in the peripheral regions of the film, while the release at later time points is influenced by the degradation of the polymer chains. The slow release of the drugs at later time points clearly indicates the surface erosion of the polymer film. PLCL polymer is known to exhibit slow hydrolytic degradation,[44] which is manifested through the slow release profiles observed in the present study.

3.4. *In vitro* Degradation. A gradual change in surface morphology of the dual drug loaded PLCL coating was observed during the degradation study (Figure 5). At initial time points, micro pores were formed in the coating indicating water penetration due to hydrolysis and release of the surface bound drug molecules. At later time points, the size of the pores was found to progressively increase due to greater permeation of water through the void spaces formed by the release of the surface entrapped drug. The burst release observed in the initial time points correlates with the release surface bound drug. As the nonpolar fenofibrate tends to localize in the interior, the burst release and subsequent

DOI: 10.1021/acsbiomaterials.9b00303
ACS Biomater. Sci. Eng. 2019, 5, 2899−2915

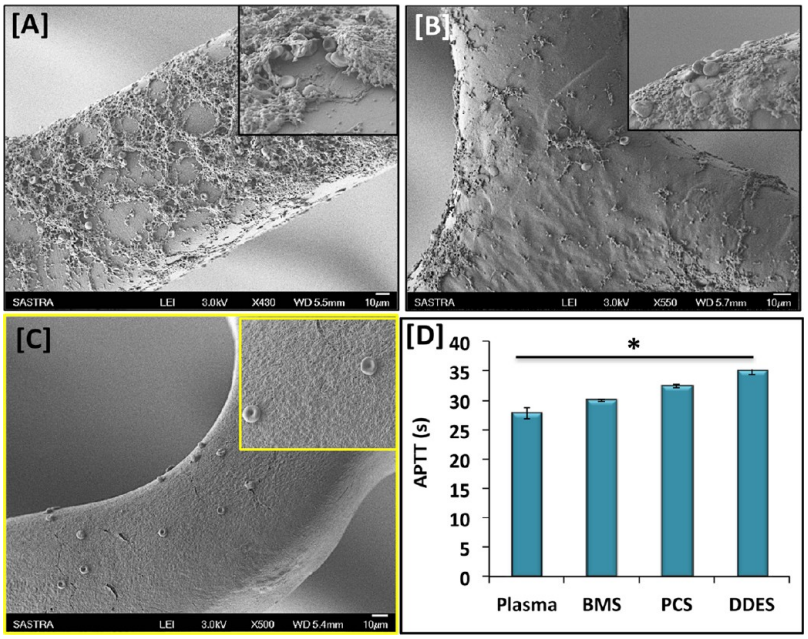

Figure 9. Scanning electron micrographs of whole blood adhesion on [A] 316S stainless steel stent, [B] polymer coated stent, and [C] dual drug-loaded PLCL coated stent. [D] Coagulation times recorded in the APTT test for different samples (*$p < 0.05$ with respect to plasma control). Scale bars represent 10 μm.

sustained release due to the surface erosion of the polymer is of lower magnitude for fenofibrate than atorvastatin. These data clearly suggest that a dominant surface erosion of the polymer coating is in operation. Similar observations have been reported by Biggs et al., wherein the relation of drug release from the drug-rich region of a commercial drug eluting stent and pore formation on the surface and micronetworks in the subsurface area of coating has been described.[43]

3.5. *In Vitro* Studies. Figure 6 shows the phase contrast images of the cells in the vicinity of the bare metal and dual drug-loaded stents. Endothelial cells cultured with bare metal and dual drug-loaded PLCL coated stent exhibit normal morphology with no visible effect on their proliferation at each time point (Figure 6). This indicates the biocompatible nature of the dual drug-loaded stent, which can aid re-endothelialization with no adverse effects on wound healing mechanism in the vascular space. In contrast, vascular smooth muscle cells show morphological changes in the presence of the dual drug-loaded stent when compared to their morphology in the presence of the bare metal stent. Smooth muscle cells surrounding the dual drug-loaded stent tend to form a contracted morphology and do not exhibit an extended shape, indicating a direct response of the cells to the drugs released in to the media (Figure 6). These results demonstrate the cytostatic effect of the combination of atorvastatin and fenofibrate on hVSMC that retard their ability to adhere and proliferate on the dual drug-loaded stent while simultaneously promoting HUVEC growth and migration.

Figure 7 shows the SEM of the HUVEC and hVSMC on the stent surface. The SEM reveals that no smooth muscle cell is adhered on the surface of dual drug-loaded PLCL coated stents. In contrast, a healthy proliferation of hVSMC on the bare metal stent was observed that progressively covers the stent surface by 72 h. This demonstrates that the dual drug-loaded PLCL coated stent inhibits the hVSMC adhesion and migration and, hence, has the potential to curb complications like restenosis. In contrast, endothelial cell adhesion was observed on the dual drug-loaded stent with an extended morphology suggesting that the dual drug combination favors the adhesion, proliferation, and extension of endothelial cells, which is beneficial for endothelialization of the stented site.

Figure 8 shows the results of immunostaining assays performed on HUVEC and hVSMC. The immunostaining assay clearly demonstrates the pleiotropic effect of atorvastatin and fenofibrate combination. Alpha smooth muscle actin staining (Figure 8) shows poor cell adhesion and negligible cell−cell communication in hVSMCs after days 1 and 3 of culture with a dual drug-loaded PLCL coated stent when compared to the bare metal stent. In contrast, CD31 (PECAM-1) staining (Figure 8) reveals a well-extended morphology of endothelial cells. The presence of the intercellular junction protein in the cells cultured on dual drug-loaded stent indicates the establishment of a cellular communication network in the endothelial cells. The immunostaining assays confirm that the drug combination promotes fast endothelialization and lowers the risk of neointimal hyperplasia through retardation of smooth muscle cell adhesion and proliferation. An earlier report has suggested that the atorvastatin and fenofibrate drug combination may exhibit a cell specific-effect on the proliferation and migration of smooth muscle cells and endothelial cells in tissue culture polystyrene culture plates.[45] Our results confirm this effect of the drug combination on a polymer-coated metal stent surface.

3.6. Whole Blood Adhesion and APTT. Figure 9 shows the blood clot formation on the bare metal stent with extensive fibrin network indicating its aggressive thrombogenic nature. This is consistent with the observation reported by earlier groups on stainless steel stents.[46] Comparatively, the polymer-coated stent shows lesser clot formation. This difference may arise due to the difference in the extent of platelet adhesion on the smooth polymer surface and their activation (Figure 9B). Interestingly, the dual drug-loaded PLCL coated stent displayed no clot formation and had significantly less red blood cells adhering to the surface. This result provides direct

DOI: 10.1021/acsbiomaterials.9b00303
ACS Biomater. Sci. Eng. 2019, 5, 2899−2915

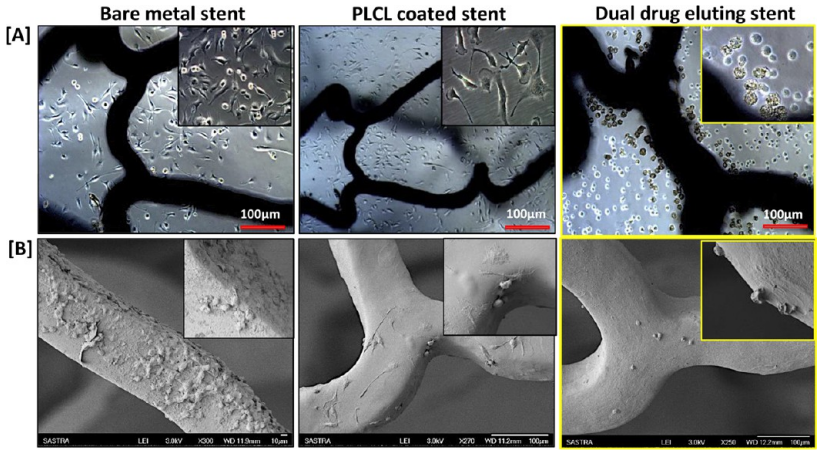

Figure 10. [A] Phase contrast images of macrophage cells in the presence of stents in culture and [B] FE-SEM of macrophages adhered to the stents after fixing.

evidence of the thromboresistant nature of the dual drug loaded PLCL coated stent (Figure 9C). The thromboresistance arises due to the pleiotropic effect of the fenofibrate and atorvastatin combination. Atorvastatin has been shown to modulate thrombomodulin levels thereby conferring thromboresistance.[47] Though no direct evidence of fenofibrate on the thrombus inhibition is available, several studies have demonstrated that fenofibrate improves endothelial function by regulating nitric oxide levels and therefore may contribute to thromboresistance indirectly.[48] Thus, the atorvastatin−fenofibrate combination in the PLCL matrix was found to be beneficial in avoiding platelet adhesion, activation, and thrombus formation. Figure 9D shows the effect of the dual drug-loaded coating on the coagulation time of platelet poor plasma (PPP) using the APTT assay. The results show a significant delay in the clotting time of PPP in the presence of a dual drug eluting stent when compared to the control indicating that the drug combination exhibits anticoagulation properties. Few earlier reports have indicated that the drug combination regulates peroxisome proliferative-activated receptors (PPARα)[49] and NADPH oxidase 2 (NOX2), which play roles in platelet activation.[50] The drugs have also been independently and in combination shown to alter the levels of coagulation factors, factor VII, fibrinogen, and PAI-1.[51] Though the exact mechanism responsible for the antithrombogenic nature of both the drugs is yet to be deciphered, it is evident that this combination possesses antithrombogenic properties through inhibition of platelet adhesion and activation that has been demonstrated in stent coatings for the first time in the present study.

3.7. Anti-inflammatory Response. Figure 10A shows the phase contrast microscopy images of LPS stimulated macrophages in culture with stent samples. The difference in the cell morphology is clearly seen in the images. In the presence of the bare metal stent, activated macrophages with dendritic morphology are observed. In the case of the PLCL coated stent, macrophages exhibit an elongated structure but are lesser in number when compared to the bare metal stent. It has been reported that the elongated phenotype of macrophages arises when the cell population possesses both M1 and M2 characteristics.[52] The M1 phenotype is considered pro-inflammatory while the M2 phenotype is anti-inflammatory.[53] The change in the macrophage phenotype in the polymer-coated stent clearly suggests a decrease in the pro-inflammatory character in the macrophages when compared with the bare metal stent. The *i*NOS (inducible nitric oxide synthase) levels in cells serve as a marker of M1 phenotype, and our earlier results obtained with the polymer film for *i*NOS levels after 1 day of culture showed significant down-regulation.[54] This result correlates with the change in morphology of the macrophages on the polymer-coated stent after 1 day of culture. However, in the case of the dual drug-loaded PLCL coated stent, the activated macrophage morphology is transformed to a spherical morphology and the number of cells was dramatically reduced with very few cells seen on the surface. These results were also confirmed by the electron micrographs recorded using FE-SEM, which reveals the change in morphology of macrophages adhered to the surface of stents (Figure 10B). These results demonstrate the anti-inflammatory character of the dual drug-loaded polymer stent coating. The combination of atorvastatin and fenofibrate have been reported for their anti-inflammatory effect on inflammatory markers like C-reactive protein, fibrinogen, and vascular cell adhesion molecule in patients suffering from diabetes and hyperlipidemia.[55−58]

Our results show the implication of these effects in the presence of the polymer matrix on the stent surface. The polymer contributes to the shift toward anti-inflammatory phenotype while the drug combination augments this effect and also prevents the adhesion of the macrophages on the stent surface. The initial burst release of the drugs has been reported to be essential to control inflammation and associated adverse effects at the stented site.[59] Therefore, the initial burst release profile is adequate for exhibiting anti-inflammatory effects. The dose-dependency of atorvastatin has been found to vary for different pleiotropic effects.[60,61] Some reports have indicated that very low concentrations of 1−15 μg/L for statin's pleiotropic effects.[60] As endothelialization is promoted on the films even in the early stages, we believe that this combination may prove to be superior even in the longer time points.

3.8. Biofilm Formation. Stent infection is a rare and life-threatening condition with a high mortality rate.[62] More than 50 cases have been reported for stent-based infections, which cause septic emboli followed by thrombosis and death.[63] *Staphylococcus aureus* is the most common and widely reported pathogen, which was also identified in the stent infections.[63] In this context, we investigated the ability of the dual drug-loaded

DOI: 10.1021/acsbiomaterials.9b00303
ACS Biomater. Sci. Eng. 2019, 5, 2899−2915

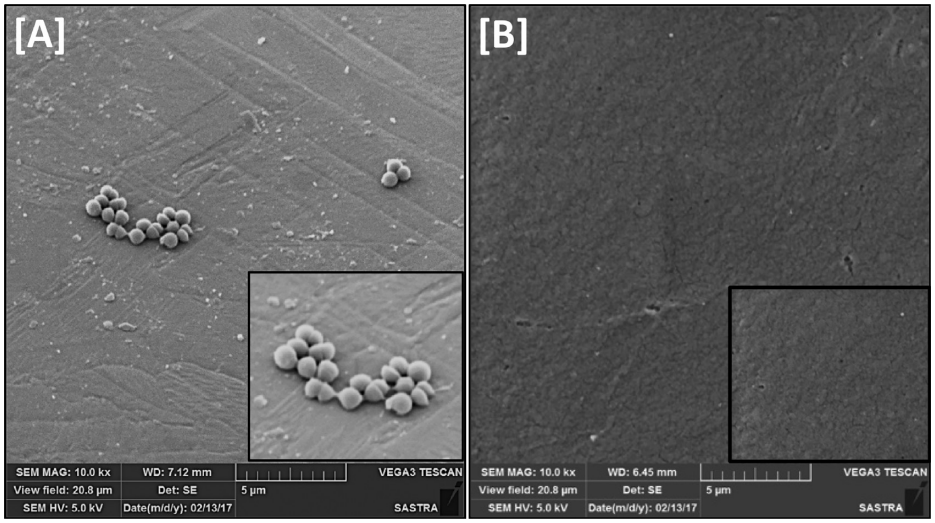

Figure 11. SEM images of [A] bare metal stent and [B] dual drug loaded stent after 24 h of culture with *Staphylococcus aureus*. Scale bars represent 5 μm.

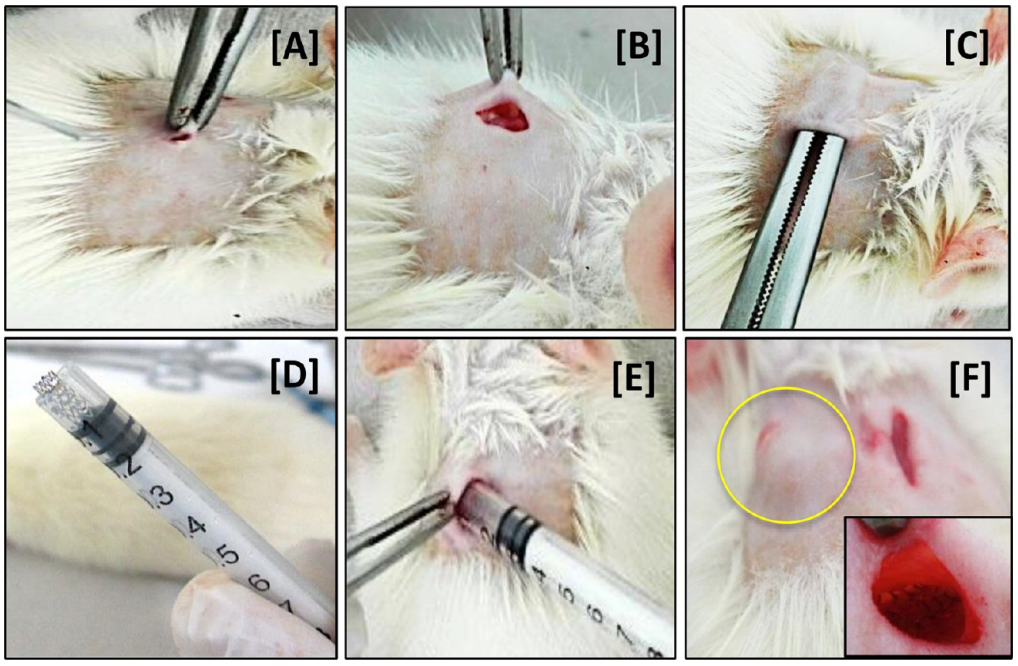

Figure 12. Representation of surgical procedure for stent implantation in subcutaneous pouch of *Wistar* rat model. [A] A superficial incision in the skin was made. [B] After dissection, the subcutaneous region is exposed. [C] A deep pocket is made using sterile surgical scissors. [D] Modified 1 mL syringe for smooth insertion of stents. [E] Implantation of stent in subcutaneous pouch. [F] Visibility of the stent under the skin is highlighted. (inset) Stent in pocket.

PLCL coated stent to inhibit biofilm formation by *Staphylococcus aureus* as direct evidence of the antibacterial effect of the drug combination. SEM images shown in Figure 11 clearly indicate the difference between the bare metal stent and dual drug-loaded stents. Few regions of the metal stent show bacterial adhesion and colony formation, which can lead to biofilm formation in the course of time. In contrast, no bacterial adhesion was discernible on the dual drug-loaded PLCL coated stent. Atorvastatin present in the combination has been reported earlier to have an antibacterial effect,[64] and this might have contributed to the inhibition of bacterial adhesion on the dual drug-loaded PLCL coated stent.

3.9. *In Vivo* Biocompatibility Studies. The subcutaneous pouch implantation is the most common method to evaluate the *in vivo* biocompatibility of biomaterials. Since the polymer coating and the drug combination employed has never been investigated earlier for stent applications, histocompatibility assessment is necessary before proceeding for further trials. Hence, subcutaneous implantation of the dual drug eluting stent was carried out in rats. A commercial single drug-eluting stent with a PLGA coating was used for comparison, and the results are presented in Figure 12. No mortality was observed in any group during the period of study, and all animals recovered completely after surgery. There was no visible inflammation in the implanted area post-stent implantation. The body weight of animals increased normally every week indicating no toxicity associated with the implantation procedure.

DOI: 10.1021/acsbiomaterials.9b00303
ACS Biomater. Sci. Eng. 2019, 5, 2899−2915

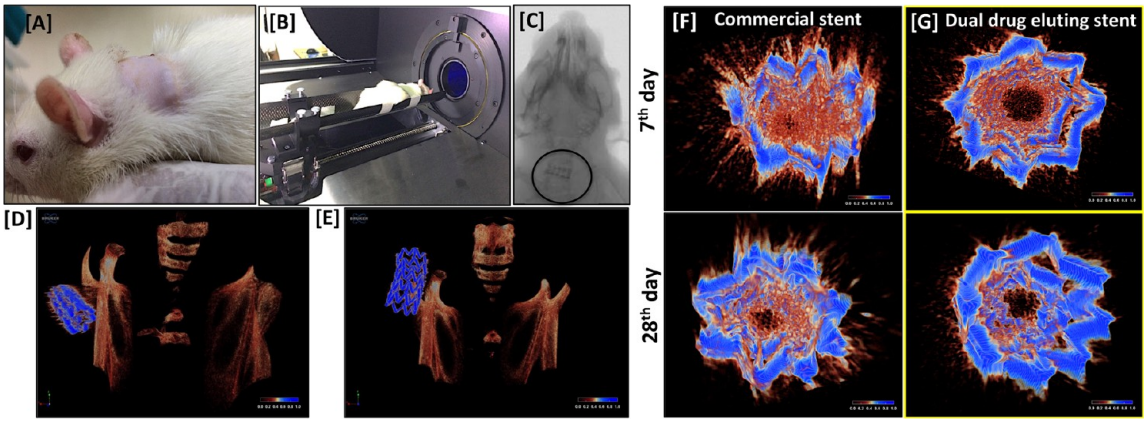

Figure 13. [A] μCT scan of an animal with a dual drug loaded PLCL coated stent. [B] The animal is anesthetized and fixed to scanning tray. [C] Scout scan of area near stent implantation. [D] Overall tissue density mapping after 1 week of stent implantation of the commercial stent and [E] dual drug eluting stent. The face-on view after density mapping of the commercial [F] and dual drug eluting stent [G] post-stenting.

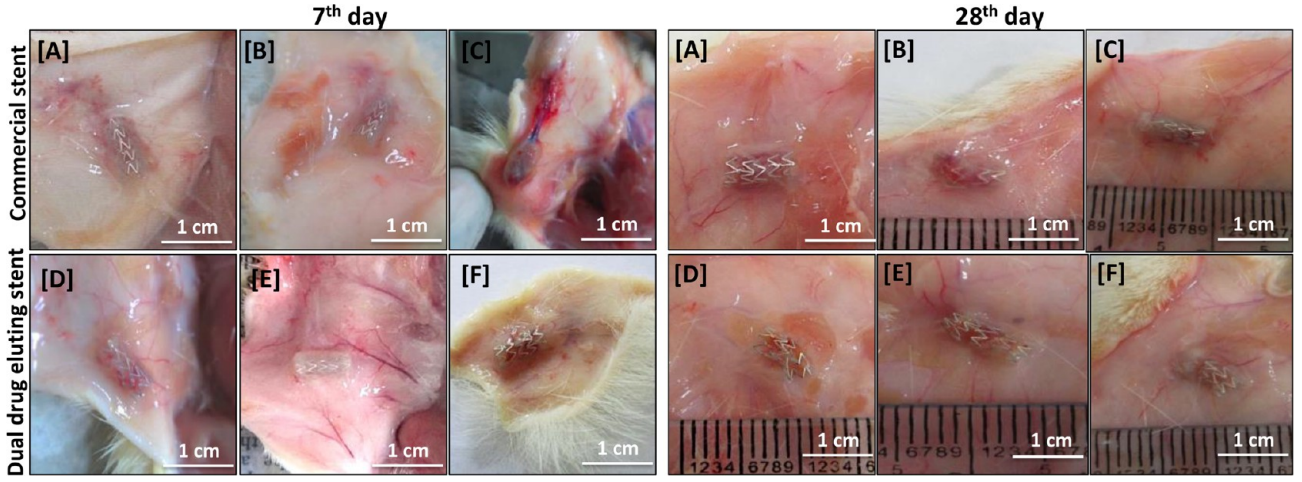

Figure 14. Optical images of commercial stents [A−C] and dual drug loaded PLCL coated stents [D−F] in the subcutaneous pocket after 7 and 28 days of implantation.

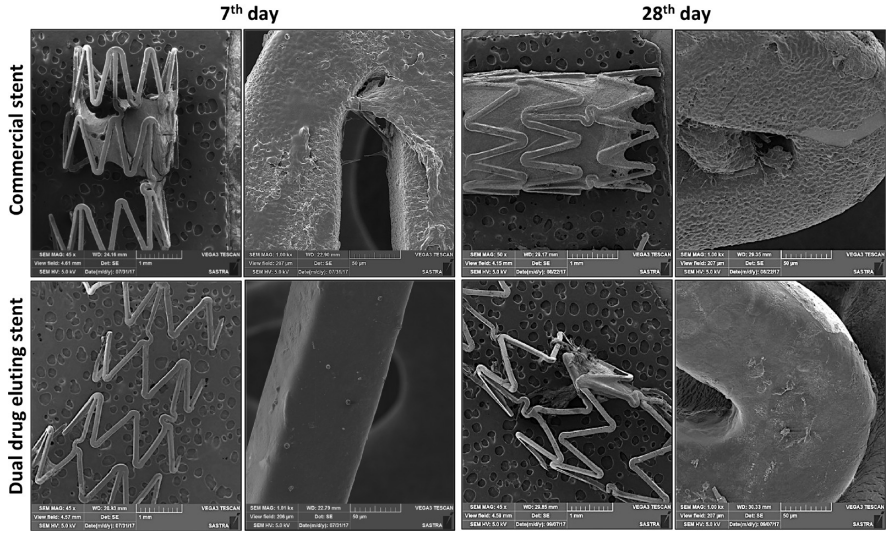

Figure 15. FE-SEM of the commercial stent and dual drug-loaded PLCL coated stent at different magnifications 7 and 28 days of post-stenting. Scale bars represent 1 mm and 50 μm.

3.10. Micro-CT Analysis. The μCT scan of the stented area and the surrounding tissue before necropsy are shown in Figure 13. The scan images were processed using 3D visualization software for identifying the signal intensities due to the metal and tissue. A greater tissue density was observed around the commercial stent when compared with the dual

DOI: 10.1021/acsbiomaterials.9b00303
ACS Biomater. Sci. Eng. 2019, 5, 2899−2915

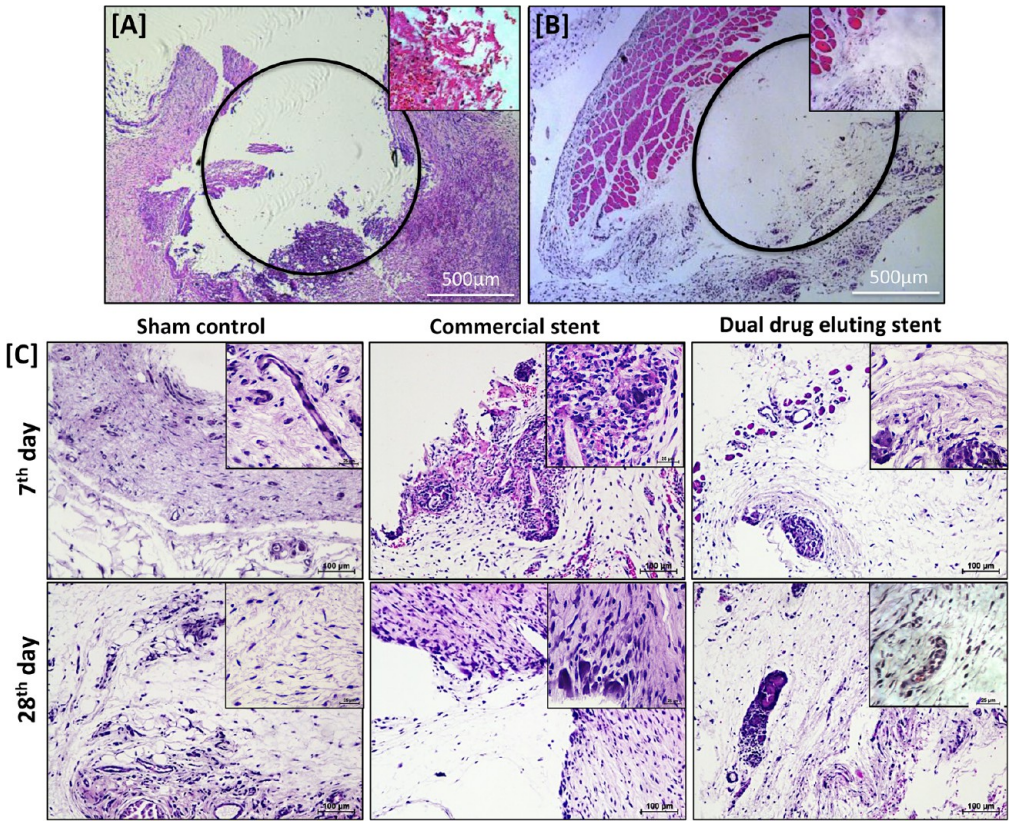

Figure 16. Optical microscopic images of push out test for H&E stained [A] commercial stent and [B] dual drug loaded PLCL coated stent with the circle indicating the position of the stent. [C] Comparison of the tissue surrounding the implants after 7 and 28 days post-stenting. The scale bar represents 100 μm.

drug-loaded PLCL coated stent at both time points (Figure 13F). The results indicate that a higher density of fibrous tissue is present around the commercial stent unlike the dual drug-loaded PLCL coated stent, which shows a lesser density of surrounding tissue. This suggests that the polymer coated dual drug loaded stent exhibits better tissue compatibility and elicits the minimal inflammatory response from the tissue that is reflected in the absence of a fibrous capsule surrounding the stent.

3.11. Necropsy. Images of implantation site taken after euthanization of the animals reveal capillary network and blood clot formation indicating severe inflammation in one animal each from the commercial stent group at both time points while the other animals in the group appeared normal (Figure 14). All dual drug loaded polymer coated stents were clearly visible in the subcutaneous pocket with no visible inflammatory response or clot formation, which is in agreement with the inferences drawn from the *in vitro* experiments.

3.12. Scanning Electron Microscopy. When the subcutaneous pouch was removed for imaging 7 days post-stenting, it was noticed that some regions in the commercial stent were highly adherent to the surrounding tissue, and at the end of the study period, the stent was found to completely adhere to the surrounding tissue. Therefore, it was processed along with tightly adhered tissue. However, the tissue surrounding the dual drug loaded PLCL coated stent was loose and was easily removed at both time points. SEM (Figure 15) revealed that the tissue covered almost half of the commercial stent. After 28 days of stenting, it is observed that the dual drug eluting stent exhibits a small amount of tissue adhesion, whereas in comparison, the commercial stents exhibit a greater amount of tissue firmly adhered to the stent. Moreover, the coating showed cracks after 28 days of stenting. These results recorded for the commercial stent may be attributed to the rough surface morphology of the coating (Supporting Information Figure S2, FE-SEM images showing surface morphology of commercial and dual drug loaded stents) that is further augmented due to the degradation of the coating. The dual drug-loaded PLCL coated stent shows very few cells adhered on the surface and the coating was relatively smooth 7 days post-stenting, which may be the reason for retarded adhesion and activation of platelets and macrophages. However, surface degradation of the coating was observed at the end of the study albeit with less tissue adhesion.

3.13. Histopathology of Tissue Surrounding the Stent. After fixing the tissue, the stent was pushed out and the surrounding tissue was stained for morphometric analysis. Figure 16A and B shows the low magnification image of the subcutaneous pouch surrounding the stent samples 7 days post-stenting. The images clearly show the accumulation of inflammatory cells surrounding the commercial stent indicating severe inflammation whereas, the tissue surrounding the dual drug-loaded PLCL coated stent appears to be normal with less inflammatory cells. Upon comparing the histological sections (Figure 16C), the commercial stent exhibited reactive fibro-vascular tissue formation as infiltration of inflammatory cells namely lymphocyte and macrophages are clearly discernible. In the case of the dual drug loaded PLCL coated stent, there was no reactive tissue formation except for a few inflammatory cells. Results from 28 days post-stenting resonate the same

DOI: 10.1021/acsbiomaterials.9b00303
ACS Biomater. Sci. Eng. 2019, 5, 2899−2915

Table 2. Histomorphometric Analysis of Tissue at the Implant Site from Different Animal Groups

	7th day			28th day		
	sham control	commercial stent	DDES	sham control	commercial stent	DDES
			Inflammation[a]			
polymorphonuclear cells	0	6	2	0	3	0
lymphocytes	15	**27**	16	18	20	16
plasma cells	1	3	4	2	5	0
macrophages	11	22	20	10	**24**	13
giant cells	0	11	1	0	**15**	7
necrosis	0	4	0	0	0	0
			Cell Type/Response[a]			
neovascularisation	1	2	1	1	1	1
fibrosis	1	2	1	1	2	1
fatty infiltrate	1	2	1	1	1	1

[a]Average over 10 images in each sample.

data with evidence of inflammation found in the commercial stent and no accumulation of inflammatory cells noted in the tissue surrounding the dual drug loaded PLCL coated stent. The results indicate that the dual drug loaded stent is least reactive with no sign of the severe inflammatory response from the subcutaneous tissue. The release of the drug combination to the surrounding tissue might have prevented the progression of inflammation as a previous study points to the anti-inflammatory activity of the drug combination.[65] However, the commercial stent displayed signs of inflammation probably due to its rough texture. It is likely that the use of a single drug may not be effective in reducing the inflammation and a drug combination could be, in comparison, more effective.

The scoring of cells performed over 10 different locations of the surrounding tissue is tabulated in Table 2. The commercial stent shows clear evidence of inflammation 28 days post-stenting indicating chronic inflammation due to the presence of the stent. The dual drug loaded PLCL coated stent exhibited low scoring for inflammatory cells when compared to the commercial stent and was comparable to the sham control 28 days post-stenting. Moreover, necrosis was observed only in the tissue surrounding the commercial stent after 7 days of stent implantation while it was absent in the tissue around the dual drug loaded PLCL coated stent. These results demonstrate the biocompatibility and safety of the novel dual drug loaded stents, which can be explored for future therapeutic studies.

3.14. Quantification of Inflammatory Cytokines. In order to quantify the magnitude of immune response, if any, elicited by the implantation of the dual drug eluting stent, cytokine quantification was performed using ELISA and the results are presented in Figure 17. The cytokine levels in the sham control were used for comparison. The results reveal that the levels of interleukin 1A (IL-1A), interleukin 1B (IL-1B), interleukin 4 (IL-4), interleukin 12 (IL-12), interleukin 13 (IL-13), interferon gamma, and granulocyte-macrophage colony stimulating factor (GM-CSF) in the serum of animals implanted with the dual drug eluting stents when compared with the sham control indicate no inflammatory response. Interestingly, the levels of interleukin 2 (IL-2), interleukin 6 (IL-6), interleukin 10 (IL-10), and RANTES were found to be significantly lower in the group implanted with the dual drug eluting stent when compared with the sham control. This indicates that the dual drug eluting stent possesses an anti-inflammatory effect that reduces the levels of pro-inflammatory cytokines. Atorvastatin has not been known to alter cytokine

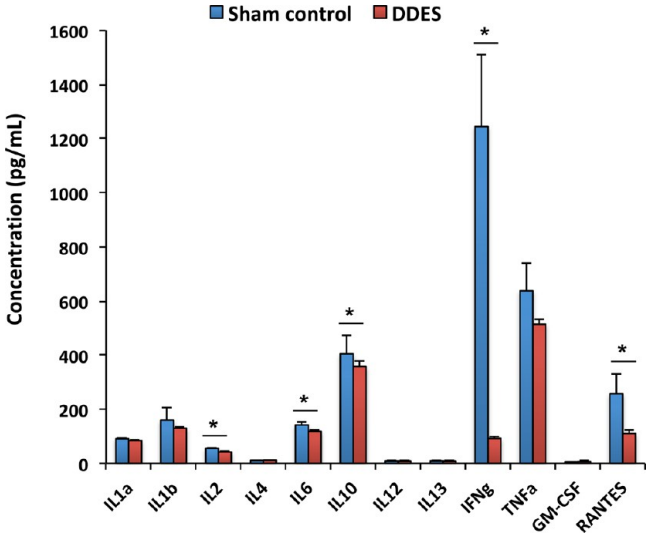

Figure 17. Quantification of inflammatory cytokines from rats 28 days after implantation using a multi-analyte ELISA kit. The concentrations are reported based on the calibration plot provided by the manufacturer.

levels according to several reports.[66] However, several studies have shown that fenofibrate can reduce the cytokine levels due to its interaction with the transcriptional regulators of NF-κB.[67] Therefore, it is evident that the presence of fenofibrate in the combination confers greater anti-inflammatory character to the dual drug eluting stent. It is also observed that the maximum decrease was observed in the pro-inflammatory cytokine RANTES in the dual drug eluting stent-implanted group (80% decrease) when compared with the sham control (52% decrease). This is because it has been recently demonstrated that both atorvastatin[68] as well as fenofibrate[69] inhibit RANTES expression, and hence, the decrease in the cytokine levels was more pronounced when compared with the others.

4. CONCLUSION

The present work has successfully employed ultrasonic spray method to fabricate a smooth and defect-free coating of dual drug loaded PLCL coating on stainless steel stent. The coating thickness of the dual drug eluting stent was found to be 1.4 μm with no peeling and cracking defects after balloon expansion. The dual drug-coated stent displayed good antithromboge-

DOI: 10.1021/acsbiomaterials.9b00303
ACS Biomater. Sci. Eng. 2019, 5, 2899−2915

nicity and anti-inflammatory properties. Biocompatibility study in *Wistar* rats also demonstrated good tissue acceptance for the dual drug loaded PLCL coated stent. The coating was stable with no inflammatory response, and the antiproliferative effect was evident in the surrounding tissue. This study has highlighted for the first time the promise of an atorvastatin−fenofibrate combination encapsulated in a polymer film as a therapeutic coating in drug eluting stents to overcome the complications associated with the present day drug eluting stents.

■ ASSOCIATED CONTENT

Supporting Information

The Supporting Information is available free of charge on the ACS Publications website at DOI: 10.1021/acsbiomaterials.9b00303.

Figures S1 and S2 (PDF)

■ AUTHOR INFORMATION

Corresponding Author

*Phone: (+91) 4362 264101 ext. 3677. Fax: (+91) 4362 264120. E-mail: umakrishnan@sastra.edu.

ORCID

Uma Maheswari Krishnan: 0000-0001-6508-4485

Notes

The authors declare no competing financial interest.

■ ACKNOWLEDGMENTS

The authors wish to acknowledge funding from the Department of Science & Technology under the FIST programme (SR/FST/LSI-453/2010) and infrastructural support from SASTRA Deemed University. P.R. gratefully acknowledges the financial assistance from SASTRA Deemed University under the TA fund. The authors also thank Ms. Preeti Vani from M/s. Sahajanand laser technology (Gujarat, India) for providing stents for the study.

■ REFERENCES

(1) Buttar, H. S.; Li, T.; Ravi, N. Prevention of cardiovascular diseases: Role of exercise, dietary interventions, obesity and smoking cessation. *Exp Clin Cardiol* **2005**, *10*, 229−249.

(2) Bønaa, K. H.; Mannsverk, J.; Wiseth, R.; Aaberge, L.; Myreng, Y.; Nygård, O.; Nilsen, D. W.; Kløw, N. E.; Uchto, M.; Trovik, T.; Bendz, B.; Stavnes, S.; Bjørnerheim, R.; Larsen, A. I.; Slette, M.; Steigen, T.; Jakobsen, O. J.; Bleie, Ø.; Fossum, E.; Hanssen, T. A.; Dahl-Eriksen, Ø.; Njølstad, I.; Rasmussen, K.; Wilsgaard, T.; Nordrehaug, J. E. Drug-Eluting or Bare-Metal Stents for Coronary Artery Disease. *N. Engl. J. Med.* **2016**, *375*, 1242−52.

(3) Celik, T.; Iyisoy, A.; Kursaklioglu, H.; Celik, M. The forgotten player of in-stent restenosis: Endothelial dysfunction. *Int. J. Cardiol.* **2008**, *126*, 443−444.

(4) Georgiadou, P.; Voudris, V. Platelet activation and stent thrombosis. *Hellenic J. Cardiol.* **2017**, *58*, 49−50.

(5) Warren, J.; Baber, U.; Mehran, R. Antiplatelet therapy after drug-eluting stent implantation. *J. Cardiol.* **2015**, *65*, 98−104.

(6) Dehmer, G. J.; Smith, K. J. Drug Eluting Coronary Artery Stents. *Am. Fam Physician* **2009**, *80*, 1245−1253.

(7) Pendyala, L. K.; Yin, X.; Li, J.; Chen, J. P.; Chronos, N.; Hou, D. The First-Generation Drug-Eluting Stents and Coronary Endothelial Dysfunction. *JACC Cardiovasc Interv.* **2009**, *2*, 1169−77.

(8) Secemsky, E. A.; Yeh, R. W.; Kereiakes, D. J.; Cutlip, D. E.; Cohen, D. J.; Steg, P. G.; Cannon, C. P.; Apruzzese, P. K.; D'Agostino, R. B., Sr; Massaro, J. M.; Mauri, L. Dual Antiplatelet Therapy (DAPT) Study Investigators. Mortality Following Cardiovascular and Bleeding Events Occurring Beyond 1 Year After Coronary Stenting: A Secondary Analysis of the Dual Antiplatelet Therapy (DAPT) Study. *JAMA Cardiol.* **2017**, *2*, 478−487.

(9) Muramatsu, T.; Onuma, Y.; Zhang, Y. J.; Bourantas, C. V.; Kharlamov, A.; Diletti, R.; Farooq, V.; Gogas, B. D.; Garg, S.; Garcıa-Garcıa, H. M.; Ozaki, Y.; Serruys, P. W. Progress in Treatment by Percutaneous Coronary Intervention: The Stent of the Future. *Rev. Esp Cardiol.(Engl Ed).* **2013**, *66*, 483−496.

(10) Harumi Higuchi Dos Santos, M.; Sharma, A.; Sun, J. L.; Pieper, K.; McMurray, J. J.; Holman, R. R.; Lopes, R. D. International Variation in Outcomes Among People with Cardiovascular Disease or Cardiovascular Risk Factors and Impaired Glucose Tolerance: Insights from the NAVIGATOR Trial. *J. Am. Heart Assoc.* **2017**, *6*, e003892.

(11) Huang, Y.; Ng, H. C.; Ng, X. W.; Subbu, V. Drug-eluting biostable and erodible stents. *J. Controlled Release* **2014**, *193*, 188−201.

(12) Herrmann, R.; Schmidmaier, G.; Märkl, B.; Resch, A.; Hähnel, I.; Stemberger, A.; Alt, E. Antithrombogenic coating of stents using a biodegradable drug delivery technology. *Thromb. Haemostasis* **1999**, *82*, 51−7.

(13) Berg, R.; Aragon, J.; Royter, V.; Shanley, J. F.; Cogert, G.; Vermani, R.; Kar, S.; Eigler, N.; Litvack, F. Pimecrolimus and dual pimecrolimus-paclitaxel eluting stents decrease neointimal proliferation in a porcine model. *Catheter Cardiovascu Interv* **2007**, *70*, 871−879.

(14) Adriaenssens, T.; Mehilli, J.; Wessely, R.; Ndrepepa, G.; Seyfarth, M.; Wieczorek, A.; Blaich, B.; Iijima, R.; Pache, J.; Kastrati, A.; Schömig, A. Does addition of estradiol improve the efficacy of a rapamycin-eluting stent? Results of the ISAR-PEACE randomized trial. *J. Am. Coll. Cardiol.* **2007**, *49*, 1265−71.

(15) Thipparaboina, R.; Khan, W.; Domb, A. J. Eluting combination drugs from stents. *Int. J. Pharm.* **2013**, *454*, 4−10.

(16) Ma, X.; Oyamada, S.; Gao, F.; Wu, T.; Robich, M. P.; Wu, H.; Wang, X.; Buchholz, B.; McCarthy, S.; Gu, Z.; Bianchi, C. F.; Sellke, F. W.; Laham, R. Paclitaxel/sirolimus combination coated drug-eluting stent: In vitro and in vivo drug release studies. *J. Pharm. Biomed. Anal.* **2011**, *54*, 807−811.

(17) Räber, L.; Serruys, P. W. Late vascular response following drug-eluting stent implantation. *JACC: Cardiovasc Interv.* **2011**, *4*, 1075−8.

(18) Han, S. H.; Quon, M. J.; Koh, K. K. Beneficial Vascular and Metabolic Effects of Peroxisome Proliferator−Activated Receptor-α Activators. *Hypertension* **2005**, *46*, 1086−1092.

(19) Ortego, M.; Bustos, C.; Hernández-Presa, M. A.; Tuñón, J.; Dıaz, C.; Hernández, G.; Egido, J. Atorvastatin reduces NF-κB activation and chemokine expression in vascular smooth muscle cells and mononuclear cells. *Atherosclerosis* **1999**, *147*, 253−261.

(20) Li, J.; Jiang, J.; Yin, H.; Wang, L.; Tian, R.; Li, H.; Wang, Z.; Li, D.; Wang, Y.; Gui, Y.; Walsh, M. P.; Zheng, X. L. Atorvastatin Inhibits Myocardin Expression in Vascular Smooth Muscle Cells. *Hypertension* **2012**, *60*, 145−153.

(21) Yin, H.; Gui, Y.; Zheng, X. L. 2-methoxyestradiol inhibits atorvastatin-induced rounding of human vascular smooth muscle cells. *J. Cell. Physiol.* **2009**, *222*, 556−564.

(22) Li, M.; Liu, Y.; Dutt, P.; Fanburg, B. L.; Toksoz, D. Inhibition of serotonin-induced mitogenesis, migration and ERK MAPK nuclear translocation in vascular smooth muscle cells by atorvastatin. *Am. J. Physiol Lung Cell Mol. Physiol* **2007**, *293*, L463−L471.

(23) Chen, S.; Liu, B.; Kong, D.; Li, S.; Li, C.; Wang, H.; Sun, Y. Atorvastatin Calcium Inhibits Phenotypic Modulation of PDGF-BB-Induced VSMCs via Down-Regulation the Akt Signaling Pathway. *PLoS One* **2015**, *10*, e0122577.

(24) Li, C. Y.; Liang, W.; Li, H.; Wang, F.; Xie, W. H. Atorvastatin inhibits PDGF-BB induced vascular smooth muscle cells proliferation and migration in cerebrovascular diseases. *Int. J. Clin Exp Med.* **2016**, *9*, 220824−220834.

(25) Zemankova, L.; Varejckova, M.; Dolezalova, E.; Fikrova, P.; Jezkova, K.; Rathouska, J.; Cerveny, L.; Botella, L. M.; Bernabeu, C.; Nemeckova, I.; Nachtigal, P. Atorvastatin-induced endothelial nitric

DOI: 10.1021/acsbiomaterials.9b00303
ACS Biomater. Sci. Eng. 2019, 5, 2899−2915

oxide synthase expression in endothelial cells is mediated by endoglin. *J. Physiol Pharmacol.* **2015**, *66*, 403−13.
(26) Xiao, H.; Qin, X.; Ping, D.; Zuo, K. Inhibition of Rho and Rac Geranylgeranylation by Atorvastatin Is Critical for Preservation of Endothelial Junction Integrity. *PLoS One* **2013**, *8*, e59233.
(27) Llevadot, J.; Asahara, T. Effects of Statins on Angiogenesis and Vasculogenesis. *Rev. Esp. Cardiol.* **2002**, *55*, 838−44.
(28) S. Antonopoulos, A.; Margaritis, M.; Lee, R.; Channon, K.; Antoniades, C. Statins as Anti-Inflammatory Agents in Atherogenesis: Molecular Mechanisms and Lessons from the Recent Clinical Trials. *Curr. Pharm. Des.* **2012**, *18*, 1519−1530.
(29) Feng, B.; Xu, L.; Wang, H.; Yan, X.; Xue, J.; Liu, F.; Hu, J. F. Atorvastatin exerts its anti-atherosclerotic effects by targeting the receptor for advanced glycation end products. *Biochim. Biophys. Acta, Mol. Basis Dis.* **2011**, *1812*, 1130−1137.
(30) Noonan, J. E.; Jenkins, A. J.; Ma, J. X.; Keech, A. C.; Wang, J. J.; Lamoureux, E. L. An Update on the Molecular Actions of Fenofibrate and Its Clinical Effects on Diabetic Retinopathy and Other Microvascular End Points in Patients With Diabetes. *Diabetes* **2013**, *62*, 3968−3975.
(31) Pascal, M.; Sepulchre, C.; Chazan, J. B.; Majoie, B. Evidence for the inhibition of platelet derived growth factor induced rat smooth muscle cells DNA synthesis by fenofibric acid at the G_0/G_1, cell cycle level. *Life Sci.* **1983**, *33*, 925−933.
(32) Nigro, J.; Ballinger, M. L.; Dilley, R. J.; Jennings, G. L. R.; Wight, T. N.; Little, P. J. Fenofibrate modifies human vascular smooth muscle proteoglycans and reduces lipoprotein binding. *Diabetologia* **2004**, *47*, 2105−2113.
(33) Lee, J. J.; Jin, Y. R.; Yu, J. Y.; Munkhtsetseg, T.; Park, E. S.; Lim, Y.; Kim, T. J.; Pyo, M. Y.; Hong, J. T.; Yoo, H. S.; Kim, Y.; Yun, Y. P. Antithrombotic and antiplatelet activities of fenofibrate, a lipid-lowering drug. *Atherosclerosis* **2009**, *206*, 375−382.
(34) Diep, Q. N.; Amiri, F.; Touyz, R. M.; Cohn, J. S.; Endemann, D.; Neves, M. F.; Schiffrin, E. L. PPARα Activator Effects on Ang II-Induced Vascular Oxidative Stress and Inflammation. *Hypertension* **2002**, *40*, 866−871.
(35) Rodriguez-Granillo, A.; Rubilar, B.; Rodriguez-Granillo, G.; Rodriguez, A. E. Advantages and disadvantages of biodegradable platforms in drug eluting stents. *World J. Cardiol.* **2011**, *3*, 84−92.
(36) Fernández, J.; Etxeberria, A.; Ugartemendia, J. M.; Petisco, S.; Sarasua, J. R. Effects of chain microstructures on mechanical behavior and aging of a poly (L-lactide-co-ε-caprolactone) biomedical thermoplastic-elastomer. *J. Mech Behav Biomed Mater.* **2012**, *12*, 29−38.
(37) Thakkar, A. S.; Dave, B. A. Revolution of drug-eluting coronary stents: an analysis of market leaders. *EMJ* **2016**, *4*, 114−125.
(38) Bose, S.; Keller, S. S.; Alstrøm, T. S.; Boisen, A.; Almdal, K. Process Optimization of Ultrasonic Spray Coating of Polymer Films. *Langmuir* **2013**, *29*, 6911−6919.
(39) Routledge, T. J.; Lidzey, D. G.; Buckley, A. B. Ultrasonic spray coating as an approach for large-area polymer OLEDs: The influence of thin film processing and surface roughness on electrical performance. *AIP Adv.* **2019**, *9*, 015330.
(40) Shanshan, C.; Lili, T.; Yingxue, T.; Bingchun, Z.; Ke, Y. Study of drug-eluting coating on metal coronary stent. *Mater. Sci. Eng., C* **2013**, *33*, 1476−1480.
(41) Mohan, A.; Narayanan, S.; Balasubramanian, G.; Sethuraman, S.; Krishnan, U. M. Dual Drug Loaded Nanoliposomal Chemotherapy: A Promising Strategy for Treatment of Head and Neck Squamous Cell Carcinoma. *Eur. J. Pharm. Biopharm.* **2016**, *99*, 73−83.
(42) Ramana, L. N.; Sharma, S.; Sethuraman, S.; Ranga, U.; Krishnan, U. M. Stealth anti-CD4 conjugated immunoliposomes with dual antiretroviral drugs − Modern Trojan horses to combat HIV. *Eur. J. Pharm. Biopharm.* **2015**, *89*, 300−11.
(43) Biggs, K. B.; Balss, K. M.; Maryanoff, C. A. Pore Networks and Polymer Rearrangement on a Drug-Eluting Stent as Revealed by Correlated Confocal Raman and Atomic Force Microscopy. *Langmuir* **2012**, *28*, 8238−8243.
(44) Jelonek, K.; Kasperczyk, J.; Li, S.; Dobrzynski, P.; Janeczek, H.; Jarzabek, B. Novel Poly(L-lactide-co-ε-caprolactone) Matrices Obtained with the Use of $Zr[Acac]_4$ as Nontoxic Initiator for Long-Term Release of Immunosuppressive Drugs. *BioMed Res. Int.* **2013**, *2013*, 607351.
(45) Giordano, A.; Romano, S.; Nappo, G.; Messina, S.; Polimeno, M.; Corcione, N.; Cali, G.; Ferraro, P.; Monaco, M.; Zambrano, N.; Romano, M. F. Atorvastatin sensitises vascular smooth muscle cells, but not endothelial cells, to TNF-α-induced cell death. *Curr. Pharm. Des.* **2012**, *18*, 6331−8.
(46) Mikhalovska, L. I.; Santin, M.; Denyer, S. P.; Lloyd, A. W.; Teer, D. G.; Field, S.; Mikhalovsky, S. V. Fibrinogen adsorption and platelet adhesion to metal and carbon coatings. *Thromb. Haemostasis* **2004**, *92*, 1032−9.
(47) Rodriguez, A. L.; Wojcik, B. M.; Wrobleski, S. K.; Myers, D. D., Jr.; Wakefield, T. W.; Diaz, J. A. Statins, inflammation and deep vein thrombosis: a systematic review. *J. Thromb. Thrombolysis* **2012**, *33*, 371−382.
(48) Westcott, C.; Genis, A.; Mthethwa, M.; Graham, R.; Van Vuuren, D.; Huisamen, B.; Strijdom, H. Fenofibrate protects endothelial cells against the harmful effects of TNF-alpha. *SAHeart* **2017**, *14*, 22−34.
(49) Ali, F. Y.; Armstrong, P. C.; Dhanji, A. R.; Tucker, A. T.; Paul-Clark, M. J.; Mitchell, J. A.; Warner, T. D. Antiplatelet Actions of Statins and Fibrates Are Mediated by PPARs. *Arterioscler., Thromb., Vasc. Biol.* **2009**, *29*, 706−711.
(50) Violi, F.; Calvieri, C.; Ferro, D.; Pignatelli, P. Statins as Antithrombotic Drugs. *Circulation* **2013**, *127*, 251−257.
(51) Kadikoylu, G.; Yukselen, V.; Yavasoglu, I.; Bolaman, Z. Hemostatic Effects of Atorvastatin Versus Simvastatin. *Ann. Pharmacother.* **2003**, *37*, 478−84.
(52) Cabanel, M.; Brand, C.; Oliveira-Nunes, M. C.; Cabral-Piccin, M. P.; Lopes, M. F.; Brito, J. M.; de Oliveira, F. L.; El-Cheikh, M. C.; Carneiro, K. Epigenetic Control of Macrophage Shape Transition towards an Atypical Elongated Phenotype by Histone Deacetylase Activity. *PLoS One* **2015**, *10*, e0132984.
(53) Liu, Y. C.; Zou, X. B.; Chai, Y. F.; Yao, Y. M. Macrophage Polarization in Inflammatory Diseases. *Int. J. Biol. Sci.* **2014**, *10*, 520−529.
(54) Roopmani, P.; Krishnan, U. M. Harnessing the pleiotropic effects of atorvastatin-fenofibrate combination for cardiovascular stents. *Mater. Sci. Eng., C* **2018**, *92*, 875−891.
(55) Hogue, J. C.; Lamarche, B.; Tremblay, A. J.; Bergeron, J.; Gagne, C.; Couture, P. Differential effect of atorvastatin and fenofibrate on plasma oxidized low-density lipoprotein, inflammation markers, and cell adhesion molecules in patients with type 2 diabetes mellitus. *Metab., Clin. Exp.* **2008**, *57*, 380−386.
(56) Tsimihodimos, V.; Kostoula, A.; Kakafika, A.; Bairaktari, E.; Tselepis, A. D.; Mikhailidis, D. P.; Elisaf, M. Effect of Fenofibrate on Serum Inflammatory Markers in Patients With High Triglyceride Values. *J. Cardiovasc. Pharmacol. Ther.* **2004**, *9*, 27−33.
(57) Wang, X. Q.; Luo, N. S.; Salah, Z. Q.; Lin, Y. Q.; Gu, M. N.; Chen, Y. X. Atorvastatin Attenuates TNF-alpha Production via Heme Oxygenase-1 Pathway in LPS-stimulated RAW264.7 Macrophages. *Biomed. Environ. Sci.* **2014**, *10*, 786−793.
(58) Paukkeri, E. L.; Leppänen, T.; Sareila, O.; Vuolteenaho, K.; Kankaanranta, H.; Moilanen, E. PPARalpha agonists inhibit nitric oxide production by enhancing iNOS degradation in LPS-treated macrophages. *Br. J. Pharmacol.* **2007**, *152*, 1081−91.
(59) Simon, D. I. Inflammation and Vascular Injury: Basic Discovery to Drug Development. *Circ. J.* **2012**, *76*, 1811−1818.
(60) Björkhem-Bergman, L.; Lindh, J. D.; Bergman, P. What is a relevant statin concentration in cell experiments claiming pleiotropic effects? *Br. J. Clin. Pharmacol.* **2011**, *72*, 164−165.
(61) Krysiak, R.; Gdula-Dymek, A.; Bachowski, R.; Okopień, B. Pleiotropic Effects of Atorvastatin and Fenofibrate in Metabolic Syndrome and Different Types of Pre-Diabetes. *Diabetes Care* **2010**, *33*, 2266−2270.

DOI: 10.1021/acsbiomaterials.9b00303
ACS Biomater. Sci. Eng. 2019, 5, 2899−2915

(62) Elieson, M.; Mixon, T.; Carpenter, J. Coronary Stent Infections-A Case Report and Literature Review. *Tex Heart Inst J.* **2012**, *39*, 884−889.
(63) Lai, C. H.; Lin, Y. K.; Lee, W. L.; Chang, W. C. Coronary Stent Infection Presented as Recurrent Stent Thrombosis. *Yonsei Med. J.* **2017**, *58*, 458−461.
(64) Ko, H. H. T.; Lareu, R. R.; Dix, B. R.; Hughes, J. D. Statins: antimicrobial resistance breakers or makers? *PeerJ* **2017**, *5*, e3952.
(65) Muhlestein, J. B.; May, H. T.; Jensen, J. R.; Horne, B. D.; Lanman, R. B.; Lavasani, F.; Wolfert, R. L.; Pearson, R. R.; Yannicelli, H. D.; Anderson, J. L. The Reduction of Inflammatory Biomarkers by Statin, Fibrate, and Combination Therapy Among Diabetic Patients With Mixed Dyslipidemia: The DIACOR (Diabetes and Combined Lipid Therapy Regimen) Study. *J. Am. Coll. Cardiol.* **2006**, *48*, 396−401.
(66) Bessler, H.; Salman, H.; Bergman, M.; Straussberg, R.; Djaldetti, M. In vitro effect of statins on cytokine production and mitogen response of human peripheral blood mononuclear cells. *Clin. Immunol.* **2005**, *117*, 73−77.
(67) Won, T. W. Fenofibrate, a peroxisome proliferator-activated receptor α-agonist, blocks lipopolysaccharide-induced inflammatory pathways in mouse liver. *Korean J. Hepatobiliary Pancreat Surg.* **2013**, *17*, 89−108.
(68) Mason, R. P.; Corbalan, J. J.; Jacob, R. F.; Dawoud, H.; Malinski, T. Atorvastatin enhanced nitric oxide release and reduced blood pressure, nitroxidative stress and reduced blood pressure, nitroxidative stress and rantes levels in hypertensive rats with diabetes. *J. Physiol. Pharmacol.* **2015**, *66*, 65−72.
(69) Feng, X.; Gao, X.; Jia, Y.; Zhang, H.; Xu, Y.; Wang, G. PPAR-α Agonist Fenofibrate Decreased RANTES Levels in Type 2 Diabetes Patients with Hypertriglyceridemia. *Med. Sci. Monit.* **2016**, *22*, 743−751.

DOI: 10.1021/acsbiomaterials.9b00303
ACS Biomater. Sci. Eng. 2019, 5, 2899−2915